Chapter-III

Direct aminocatalytic asymmetric synthesis of indolyl-piperidine from glutaraldehyde and imines

3.1 Introduction:

Among the carbon-carbon bond-building reactions, the Mannich asymmetric response is one of the most potent paths to the design of nitrogen-containing compounds.[1-7]Indole and its derivatives are very precious because of their broad spectrum of biological, synthetic, pharmaceutical activity, and cure of several diseases **(Figure 3.1)**.[8]

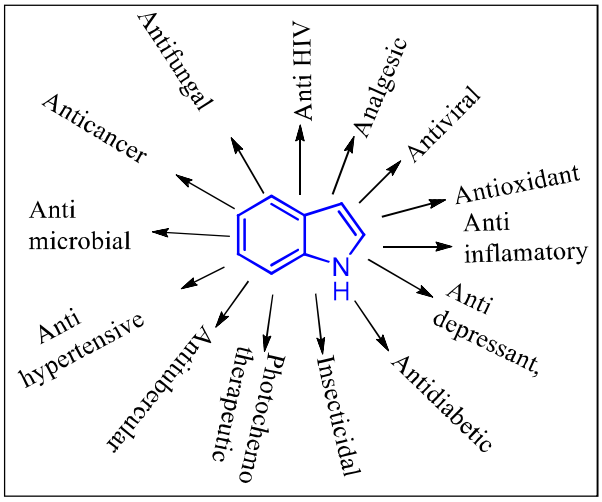

Figure 3.1 Representing the biological application of indole and indole derivatives.

The chemistry of indole has been of increasing interest since several compounds of this type possess diverse biological activities.[9] Indole derivatives are found abundantly in a variety of natural plants and exhibit various physiological properties.[10,11] These derivatives exhibit antibacterial, antifungal,[12] and antitumor activities[13]. Some of the indole alkaloids extracted from plants possess interesting cytotoxic and antiparasitic properties.[14,15] Alkaloids containing the piperidine nucleus exhibited a promising wide range of biological activities such as antimicrobial, antiparasitic, cytotoxicity, anti-inflammatory, pesticidal, and anti-HIV-1 properties. [16,17] Some piperidine derivatives are also used as neuroleptic agents.[18] Numerous bioactive compounds such as natural products, alkaloids, potent drug candidates, modern medications encompass indole fragments tethered saturated nitrogen heterocycles as crucial structural elements.[19-22] In the last decade, nitrogen heterocycles hold enormous practical utilities; in particular, more the 12,000 compounds are known that decorated with pyrrolidine and piperidine units. Consequently, indole-based heterocycles are broadly considered as "privileged motifs" exploited in medicinal as well as pharmaceutical industries,[23] even in living organism indole is present in proteins in the form of an amino acid called tryptophan. Literature reports have disclosed that indoles having a chiral functional group at its third position imparts

the biological activity, found in several pharmaceutical compounds, such as hamacenthine B represent cytotoxic activity,[24] BSM-599726 is selective serotonin reuptake inhibitor,[25] hepaendole D antimycotic and antibacterial activity.[26] Dual-action migraine drug prototype[27] Isatisine-A was isolated in 2007 from the leaves of Isatis indigotica Fort[28] and utilized to cure viral maladies such as mumps pneumonia, hepatitis, and viral influenza **(Figure 3.2)**.[29]

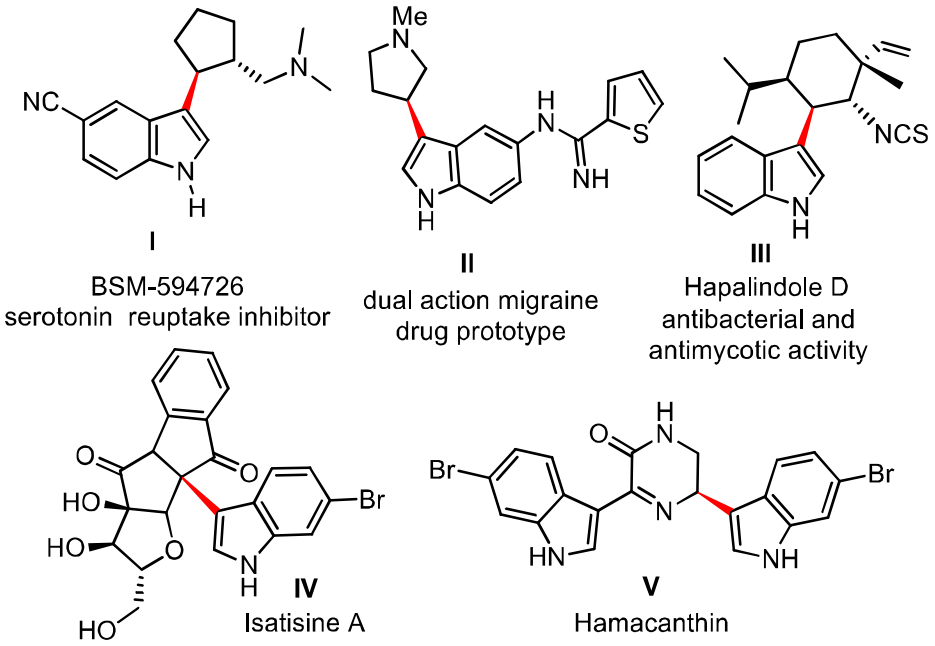

Figure 3.2 Bioactive indole based scaffold with chirality at the C-3 carbon

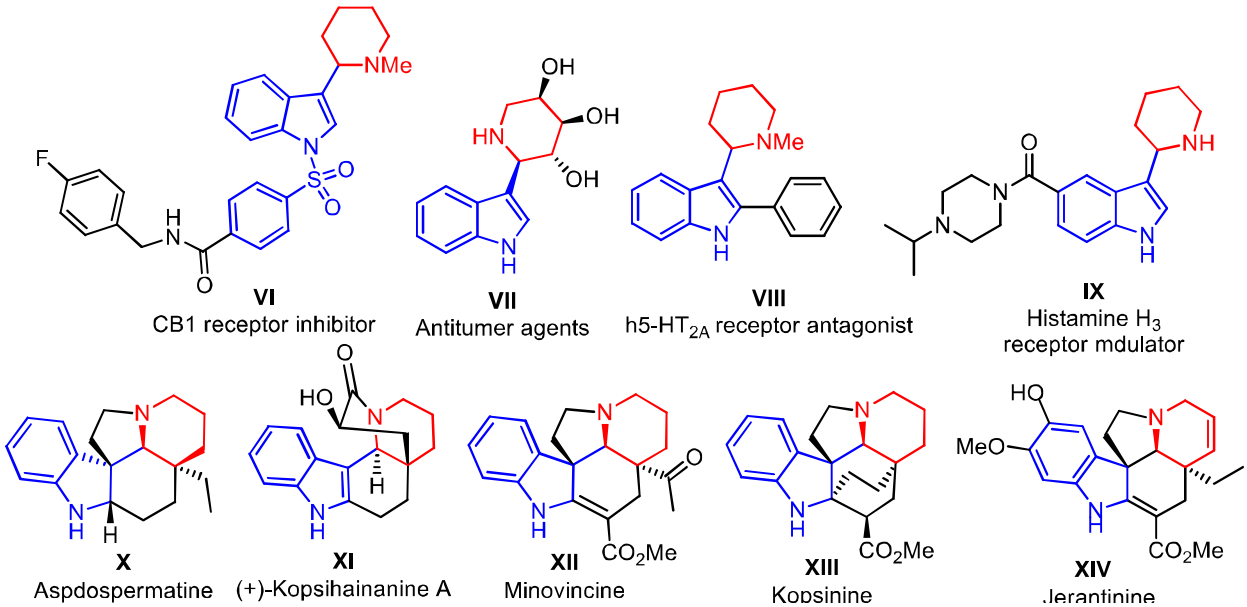

Figure 3.3 Selected bioactive indolyl-3-piperidine based compounds

Besides, indole-3-piperidine also presents as a core framework in many naturally occurring indole alkaloids, e.g., Jerantinine, Aspidosperma, Aspdospermatine, Kopsihainanine A, Vindoline Aspidoserma, Vindolinne, Minovincine which is usual structural found among several high-profile natural products derived from the Aspidosperma Kopsinine **(Figure 3.3)**.[30-38]

The chirality tethered at the C-3 carbon of indole scaffold **3** is of great interest, as discussed earlier, and there are two easy ways to access chirality at the C-3 position of indole. In the first **Path-I,** indole attack as nucleophile on the preformed imine, whereas, in **Path-II** nucleophile addition on indole based imine to access indole-moiety having a chiral center at C3-position as shown in **Scheme 3.1.**

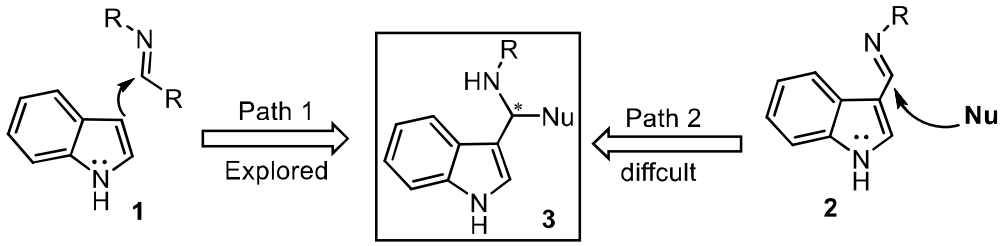

Scheme 3.1 Representation of two ways to access chirality at C-3 of indole

In this direction, Xie and co-workers have developed the synthesis of indolyl-3-piperidine involving acid-catalyzed Mannich reaction of indole with aliphatic cyclic imine tetrahydro-piperidine via **Path-I** as shown in **Scheme 3.2**.[39] This procedure does not build piperidine units on indole, instead of that just joined the preform six-membered nitrogen heterocycle, presently in the form of the cyclic imine, with indole.

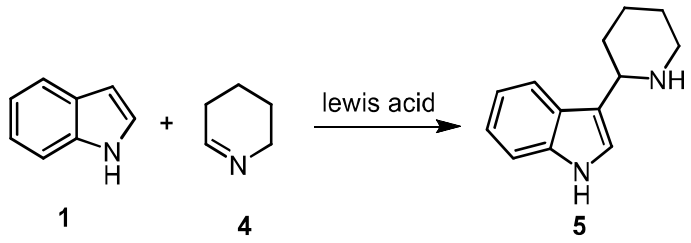

Scheme 3.2 Liang-hui approach for the synthesis of indolyl-3-piperidine

Having realized the importance of **Path-II** for the synthesis of indole-piperidine through generating the chirality at the C3-position, we understood that generating the chirality at this position is difficult as the generated chiral center undergoes elimination to furnish α,β-unsaturated compounds due to the stability of the allylic-carbocation. This phenomenon was understood through the proline-catalyzed direct Aldol reaction of N-Ts indole-3-carboxaldehyde,

and the direct Mannich reaction of N-Ts indole-3-imines with acetone, in which we got to achieve the α,β-unsaturated compound **7** as final product instead of getting direct aldol/Mannich product, since the intermediates **(i)** and **(ii)** underwent a fast elimination reaction in the same reaction conditions as shown in (Eq. (1), **Scheme 3.3**).

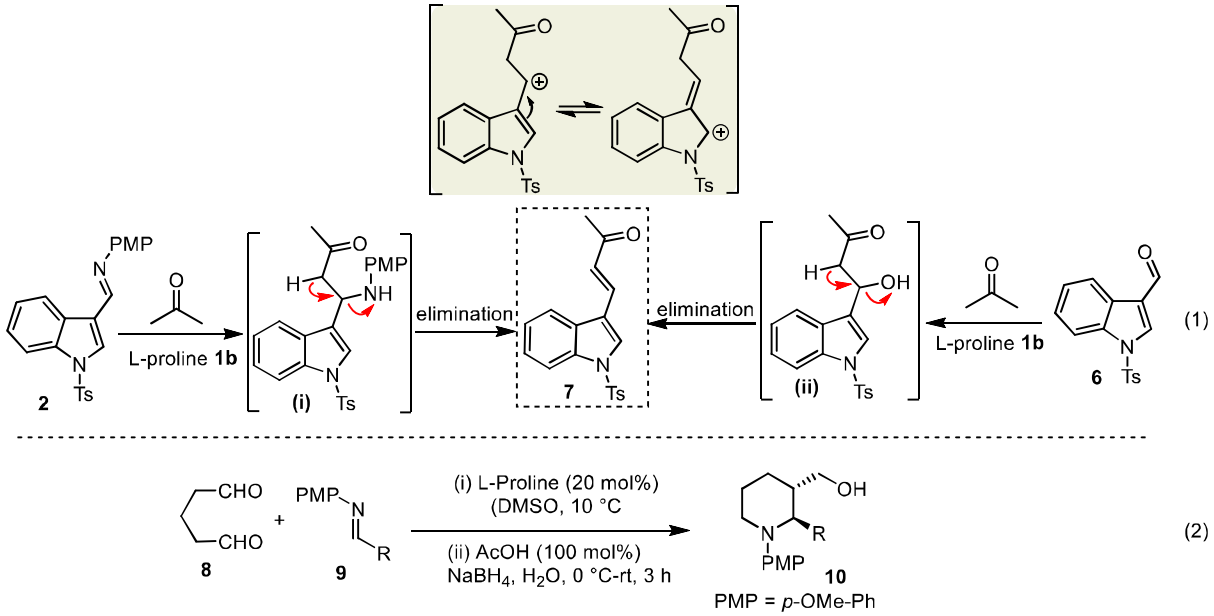

Scheme 3.3 (1) Indolyl-3-α,β-unsaturated ketone as an outcome for direct Aldol/Mannich reaction of indole-3-aldehyde or imine with acetone, (2) recently developed [4+2] annulation for the piperidine **10** synthesis

To address this issue of generating the chirality at the C3-position of indole, we plan to tarp the intermediates (i) with an internal electrophile in an intramolecular fashion, so that immediate elimination can be prohibited. In this direction, we recently developed a simple amine-catalyzed protocol for the direct asymmetric synthesis of 2,3-disubstituted piperidine through [4+2] annulation between difference aryl-imines and glutaraldehyde in one-pot fashion (Eq. 2, **Scheme 3.3**).[40] Therefore, having the importance of indole-based piperidine compounds in mind, we plan to extend this approach for the synthesis of these compounds through Path-II of Scheme 3.1. The utilization of indole-3-substituted as a suitable electrophile, due to the said problems, have not been explored for direct organocatalytic transformations. The direct organocatalytic Mannich reaction involving indole-3-imines with glutaraldehyde as a reaction precursor may provide a fascinating and innovative route to synthesize functionalized indole tethered chiral piperidine in one-pot fashion. To test our hypothesis, we initially plan to utilize of indole-3-imines as suitable substrates for the direct Mannich-reaction followed by reductive cyclization as overall [4+2]

annulation with glutaraldehyde under amine-catalysis. The standardization of the initial reaction conditions is shown in Table 3.1.

3.2 Results and discussion

In our efforts towards the integration of *N*-heterocyclic compounds [39,41-43] here we utilize glutaraldehyde **9**, as a suitable bi-functionalized compound, with several indole-3-imines **2** for the direct organocatalytic [4+2] annulation to access indole based piperidine as shown in **Table 3.1**. Having experience in this context, we quickly optimized the designed transformation by taking indole-3-imine **2a** as a model substrate with glutaraldehyde **9** and by using various amine-catalysts **1,** followed by intramolecular reductive cyclization with $NaBH_4$ afford indol-3-yl-piperidine in one-pot operation **(Table 3.1).** In our initial experimental studies in DMSO, as our choice of solvent, we tried our earlier developed condition and obtained **11a** with 48% yield **(entry 1, Table 3.1)** and with high enantioselectivity (er = 92:8). Further, attempts were made to improve the yields by changing solvents and temperature; however, reaction yield could not be improved (**entry 2,3,4, Table 3.1)**. Next, we tried the combination of DMSO: $CHCl_3$ (5:1) as solvent at room temperature in the presence of ethylene glycol or benzoic acid as an additive respectively, and product **11a** was obtained with 45% or 53% yield, respectively **(entry 5, 6, Table 3.1).** After reducing the proportion of DMSO: $CHCl_3$ from (5:1) to (3:1) with acetic acid as an additive at rt, an improvement in the reaction yield (62%) was observed **(Entry 7, Table 3.1).** Next, ethylene glycol was tested as an additive for this reaction at the same temperature and **12a** with obtained with good yield 71% **(Entry 8, Table 3.1).** Additional efforts were made to improve the reaction yield by decreasing the reaction temperature up to 0 °C in the absence of additively and **11a** was with high yield (79%) and with an excellent enantiomeric ratio (er >99:1) **(entry 9, Table 3.1)**. Next, changing the amine-catalytic system **1b-1d (entry 10, 11, 12, Table 3.1)** could not provide an increment in yield and enantiomeric ratio. Therefore, we prefer to perform this one-pot sequential methodology with the optimized conditions **(entry 9, Table 3.1)**. Further, we examined the generality of the developed protocol with several N-protected indole-3-imines, and results are summarized in **Table 3.2**. Several N-protections were carried out, but transformation worked well when imines were having tosyl, Boc, Ms, and SO_2Ph protecting group at the nitrogen of the indole nucleus. Initially, we examined N-Ts indole imines for the developed method, and the right level of yields (up to 79%) and excellent enantiomeric ratio (>99:1 er) were obtained in case of piperidine **11a-11e (entry 11a-11e, Table 3.2).** Although the

yield was quite good for all N-Ts protected indol-3-imines; however, the replacement of N-Ts-group with N-Ms-group in indolyl-imines slightly lowered the reaction yields and comparable enantiomeric ratio (up to 94:6) of functionalized Indol-3-yl piperidine **(entry 11f-11i, Table 3.2).** We also used N-Boc (**entry 11j, 11k, Table 3.2**) N-SO_2Ph (**entry 11l, 11m, Table 3.2**) with various substituted indoles. Other N-benzoyl or N-allyl, N-Cbz-protected indole imines, could not furnish the desired product under optimized conditions **(entry 11n-11p Table 3.2)**. Besides, N-Tosyl-2-methylindole imine also could not generate any desired product **(11q, Table 3.2)**.

Table 3.1 Optimization of reaction conditions [a]

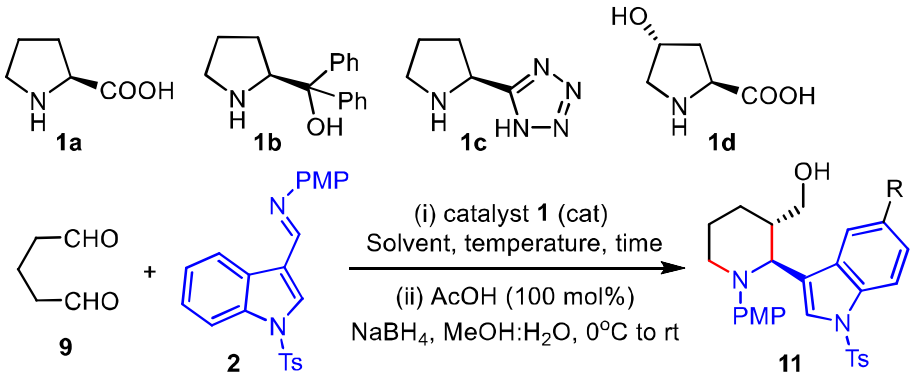

entry	cat.	solvent/condition[a]	additive[b]	time (h)[c]	yield (%)[d]	er[e]
1	**1a**	DMSO, 10 °C	-	12	48	92:8
2	**1a**	DMF, rt	-	15	28	nd
3	**1a**	Dioxane, rt	-	19	19	nd
4	**1a**	CH_3CN, rt	-	16	25	80:20
5	**1a**	DMSO:CH_3CN (5:1), rt	Ethylene glycol	15	45	80:20
6	**1a**	DMSO:$CHCl_3$ (5:1), rt	$PhCO_2H$	14	53	80:20
7	**1a**	DMSO:CH_3CN (3:1), rt	CH_3CO_2H	15	62	85:15
8	**1a**	DMSO:$CHCl_3$ (3:1), rt	Ethylene glycol	14	72	86:14
9	**1a**	DMSO:$CHCl_3$ (3:1), 0 °C	-	24	79	>99:1
10	**1b**	DMSO:$CHCl_3$ (3:1), 0 °C	-	24	45	88:12
11	**1c**	DMSO:$CHCl_3$ (3:1), 0 °C	-	24	36	89:11
12	**1d**	DMSO:$CHCl_3$ (3:1), 0 °C	-	26	43	90:10

[a](i) Imine **2** (0.3 mmol), **9** (extracted, dry over Na_2SO_4, 0.9 mmol), catalyst **1** (20 mol%), solvent (3.0 mL). [b]isolated yield after two steps in one-pot operation. [c]reaction time (h). [d]yield (%). [e]Determined by HPLC analysis using a CHIRALPAK-IC column using iPrOH–hexane as solvents.

Table 3.2 Optimization of reaction conditions[a]

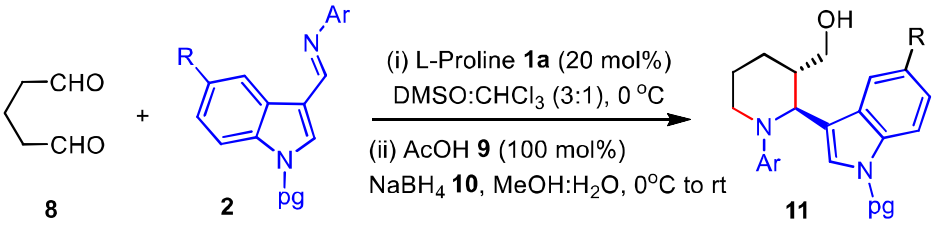

8 2 11

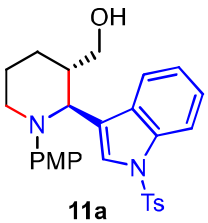

11a
79% yield
99.8:0.2 er

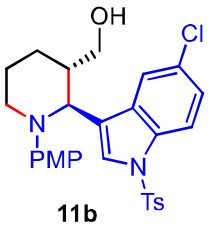

11b
71% yield
97 : 3 er

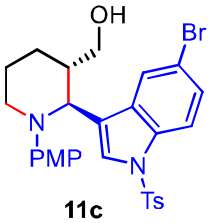

11c
72% yield
97.5: 2.5 er

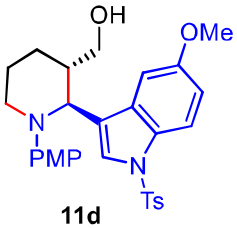

11d
75 % yield
99.6:0.4 er

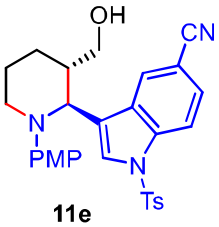

11e
65 %
yield
99:1 er

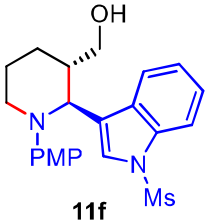

11f
70 % yield
89.5:10.5 er

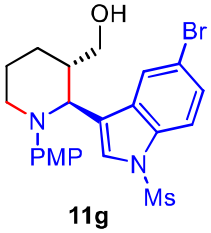

11g
62% yield
90:10 er

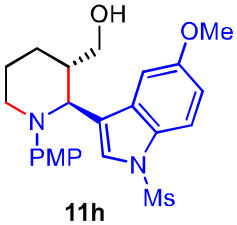

11h
68 % yield,
93.8:6.2 er

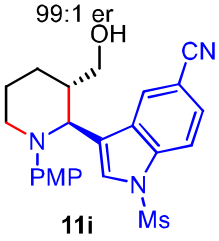

11i
67% yield
92.6:7.4 er

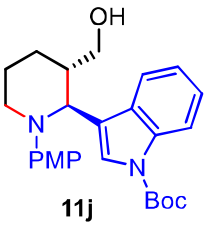

11j
64% yield
99.57:0.43 er

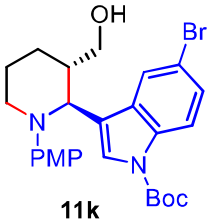

11k
66% yield
99.2:0.8 er

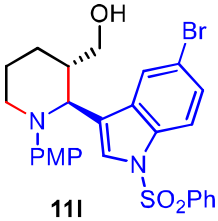

11l
64% yield
96.92:3.08 er

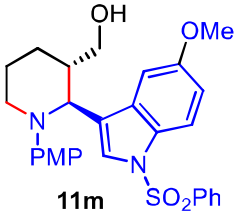

11m
68% yield
95: 5 er

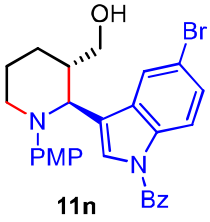

11n
nr

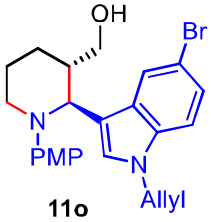

11o
nr

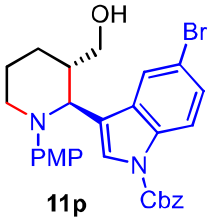

11p
nr

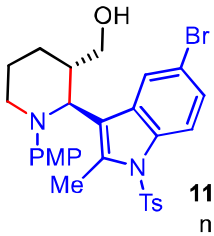

11q
nr

[a](i) Imine **2** (0.3 mmol), Glutaraldehyde **8** (extracted, dry over Na_2SO_4, 0.9 mmol), catalyst **1** (20 mol%), DMSO:$CHCl_3$ (3:1) (3.0 mL), 24 h. [b]isolated yield after two steps in the one-pot operation. [c]yield (%). [d]Determined by HPLC analysis using a CHIRALPAK-IC column using iPrOH–hexane as solvents.

3.3 Plausible mechanism for the protocol

Based on the literature report in this direction, we have proposed a tentative resection mechanism for enantioselective synthesis of indolyl-3-piperidine. This reaction proceeds through the proline-catalyzed direct Mannich reaction between through enamine intermediate **12**, in situ generated from glutaraldehyde **9**, with indole imine **2,** followed by intramolecular cyclization to the cyclic enamine as THP-intermediate **15**, which underwent acid-mediated reduction to the functionalized piperidine **11** in the same pot, as shown in **Scheme 3.3**.

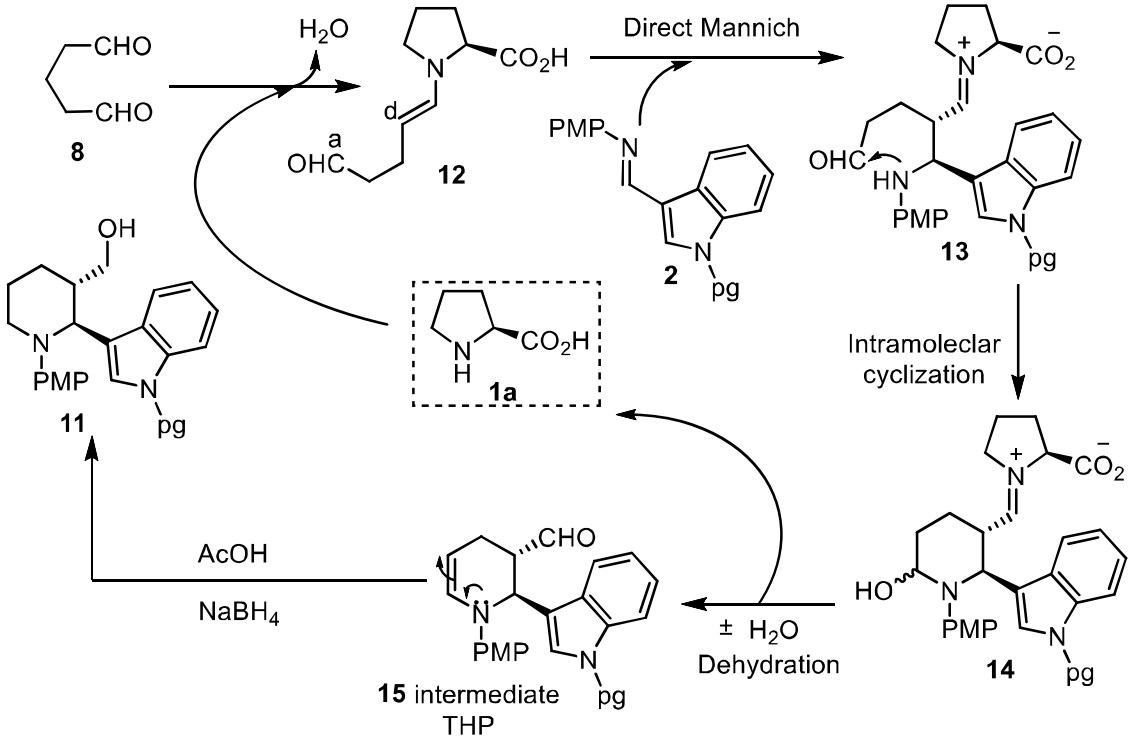

Scheme 3.3 Plausible mechanism for the synthesis of indolyl-piperidines from glutaraldehyde and indole imine

The relative stereochemistry as *trans* and absolute stereochemistry as (2S,3S) have been confirmed through a single-crystal X-ray diffraction analysis of **11g (Figure 3.6)**.

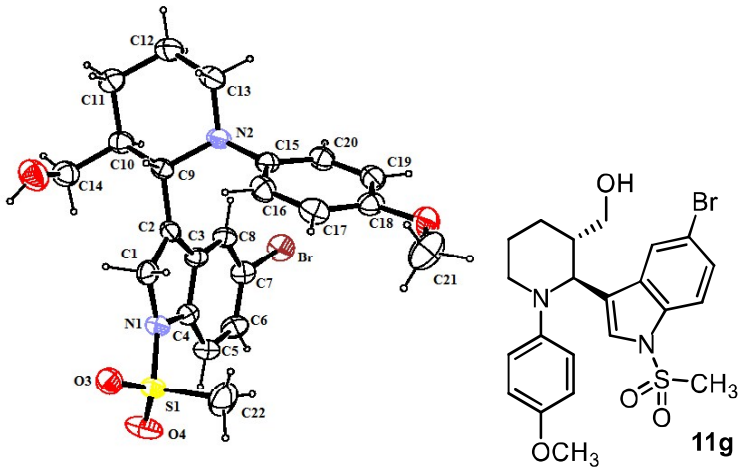

Figure 3.6 Single-crystal X-ray analysis of **11g**

3.4.1 *In-vitro* HIV-1 RT inhibitory assay

Synthesized compounds were *in-vitro* evaluated for HIV-1 RT inhibitory activity using ELISA based test following the kit protocol (Roche diagnostics). Marketed drug efavirenz was used as reference positive control during the study, and 2.5% DMSO (Sigma-Aldrich) in lysis buffer was taken as a negative control. The procedure followed is briefly described here; the reaction mixture was set with RT enzyme, template primer complex, and dNTPs in a lysis buffer with or without inhibitors and then incubated at 37 °C for 1h. Further, the mixture was transferred to a streptavidin-coated microtitre plate (MTP) and again incubated at 37 °C for 1 h. The biotin-labeled dNTPs that were incorporated in the template due to activity of RT, bound to streptavidin while unbound dNTPs were washed using wash buffer. The anti-DIG-POD was added to the MTP in the specified concentration, followed by incubation of 1 h at 37 °C. The DIG-labeled dNTPs incorporated in the template were bound to an anti-DIG-POD antibody. The unbound anti-DIG-POD was rewashed with a washing buffer, and the peroxide substrate (ABST) was added to the MTP. A colored reaction product was produced due to the cleavage of the substrate catalyzed by the peroxide enzyme. The absorbance of the sample was determined as an optical density (OD) at 405 nm using a microtiter plate ELISA reader [44, 45]. The final value of OD taken was an average of duplicate results, and %inhibition of HIV-1 RT was calculated using the below-mentioned formula

Table 3.3 HIV activity of compound **11** with respect to efavirenz

$$\% \text{ Inhibition} = 100 - \left(\frac{\text{OD at 405 nm with inhibitor}}{\text{OD at 405 nm without inhibitor}} \times 100\right)$$

Sr. No.	Compound Code	% Inhibition of HIV-1 RT activity
1.	11a	63.87
2.	11b	54.82
3.	11c	34.58
4.	11d	41.38
5.	11e	57.14
6.	11f	37.26
7.	11g	46.58
8.	11h	66.27
9.	11i	68.67
10.	11j	70.16
11.	11k	45.25
12.	11l	28.48
13.	11m	42.24
14.	**Efavirenz**	**99.86**

3.4.2 Results and Discussion

Among the titled screened compounds, analog **11j** showed the highest % inhibition of HIV-1 RT at the tested concentration. Analogs **11a, 11h, 11i** exhibited significant % inhibition of HIV-1RT and **11b, 11d, 11e, 11g, 11k, 11m** inhibited the HIV-1 RT moderately in comparison with the standard drug efavirenz. Rest all the titled compounds (**11c, 11f, 11l**) showed weak inhibition of HIV-1 RT at their respective tested concentration. In general, the compounds with unsubstituted indole nucleus (**11j, 11a**), analogs with electron-donating groups (**11h**) substituted at the phenyl ring of the indole nucleus possess significant HIV-1 RT inhibition. Apart from this, majorly, the compounds with electron-withdrawing groups (**11b, 11e, 11g, 11k, 11c, 11l**) substituted at the phenyl ring of the indole nucleus possess moderate to weak inhibition of HIV-1 RT.

3.5. *In-silico* and *in-vitro* studies of novel indole derivatives as HIV-1 RT inhibitors

3.5.1 Materials and methods

Simulation studies were carried out using Schrodinger software[46] (Version 2019-1, Schrodinger) installed on Intel Xenon W 3565 processor and Ubuntu enterprise version 18.04 as the operating system. Designed ligands were sketched in ChemDraw 18.0, Perkinelmer software. The ligands imported into the workstation of Schrodinger software and the result of the docking results were analyzed with the help of XP Visualiser (Version 2019-1, Schrodinger). QikProp[47] tool was used for the prediction of ADME (Absorption, Distribution, Metabolism, and Excretion) properties.

3.5.2 Ligand preparation

The ligands used as inputs for docking were sketched by using ChemDraw software and cleaned up the structure for the bond alignment, ligands were incorporated into the workstation and the energy minimized by using OPLS3e (Optimized Potentials for Liquid Simulations)[48] force field in Ligprep[49] (Version 2019-1, Schrodinger). This minimization helps to assign bond orders, the addition of the hydrogens to the ligands, and conversion of 2D to 3D structure for the docking studies. The generated output file (Best conformations of the ligands) was used for docking studies.

3.5.3 Receptor grid generation

A receptor grid made around the protein by choosing the inhibitory ligand (X-ray pose of the ligand in the protein). The centroid of the ligand is selected to create a grid box around it, and the Vander-Waal radius of receptor atoms was scaled to 1.00 Å with a partial atomic charge of 0.25.

3.5.4 Protein preparation

Protein was retrieved from Protein data bank (https://www.rcsb.org/structure/3mee)[50] and imported into the Protein preparation wizard[51] (Version 2019-1, Schrodinger) is the Schrodinger software, to prepare the protein and to minimize the protein. Hydrogen atom was added to the proteins, and charges were assigned. Generated Het states using Epik at pH 7.0 ±2.0. Preprocess the protein and refine, modify the protein by analyzing the workspace water molecules, and other heteroatoms. There is no water molecule in the protein. Finally, the protein minimized by using OPLS3e forcefield. A grid was created by considering cocrystal ligand, which includes the active site of the protein of the selected target (PDB-3MEE)[52]. After the final step of docking with the

cocrystal ligand in XP mode, root means square deviation (RMSD) was checked to validate the protein.

3.5.5 Docking studies

Docking studies of the designed and the synthesized compound was performed by using the Glide module[53] in Schrodinger. All docking calculations were executed by using Extra Precision (XP) mode. A scaling factor of 0.8 and a partial atomic charge of less than 0.15 was applied to the atoms of the protein. Glide docking score was used to determine the best-docked structure from the output. The interactions of these docked complexes were investigated further by using XP visualizer for the detail interactions of the ligand with amino-acid residues and water molecules.

3.5.6 *In silico* prediction of Physico-chemical parameters

Physicochemical parameters of the designed compounds were *in-silico* predicted using the Qik-prop module of Schrödinger[47]. The different parameters predicted were[54]; molecular weight (M. Wt.), total solvent accessible surface area (SASA), number of hydrogen bond donor (HBD), number of hydrogen bond acceptor (HBA), octanol/water partition coefficient (log P), aqueous solubility (Log S), predicted apparent Caco-2 cell permeability in nm/sec (PCaco) and number of rotatable bonds (Rot).

Table-3.4 Ideal range of drug-likeness parameters followed by approved drugs

1	Molecular weight (Mol wt.)	130-725
2	Total solvent accessible surface area in square angstroms (SASA)	300-1000
3	No. of hydrogen bond donor groups (HBD)	0- 6
4	No. of hydrogen bond acceptor groups (HBA)	2 to 20
5	Octanol/water partition coefficient (logP)	-2.0 to 6.5
6	Aqueous solubility, in mol dm^{-3} (logS)	–6.5 to 0.5
7	Apparent Caco-2 cell permeability in nm/sec (PCaco)	<25 poor, > 500 high
8	Brain/blood partition coefficient (logBB)	–3.0 to 1.2
9	No. of rotatable bonds (Rot)	0 to 15

Code	MW[a]	SASA[b]	donorHB[c]	accptHB[d]	logPo/w[e]	logS[f]	PCaco[g]	logBB[h]	Rotor[i]
11a.mol	490.62	768.31	1.00	7.95	4.89	-6.44	1435.68	-0.63	5.00
11b.mol	525.06	790.69	1.00	7.95	5.37	-7.14	1441.69	-0.48	5.00
11c.mol	569.51	795.55	1.00	7.95	5.45	-7.25	1442.01	-0.47	5.00
11d.mol	520.64	716.95	1.00	8.70	4.36	-5.09	914.58	-0.76	6.00
11e.mol	515.63	732.45	1.00	9.45	3.62	-6.07	219.22	-1.40	6.00
11f.mol	414.52	663.66	1.00	7.95	3.32	-4.85	1075.12	-0.63	4.00
11g.mol	493.41	691.46	1.00	7.95	3.88	-5.59	1079.88	-0.47	4.00
11h.mol	444.55	683.06	1.00	8.70	3.28	-4.67	902.60	-0.76	5.00
11i.mol	439.53	692.95	1.00	9.45	2.46	-5.56	187.29	-1.48	5.00
11j.mol	436.55	753.89	1.00	5.95	5.40	-7.12	2105.84	-0.41	4.00
11k.mol	515.45	813.06	1.00	5.95	6.16	-8.50	2186.17	-0.26	4.00
11l.mol	555.49	759.41	1.00	7.95	5.05	-6.60	1000.49	-0.60	5.00
11m.mol	506.62	698.59	1.00	8.70	4.11	-4.78	923.35	-0.75	6.00

Table-3.5 predicted Physico-chemical parameters of the title compounds

[a]MWt- Molecular weight

[b]SASA-Solvent accessible surface area

[c]HBD-No. of hydrogen bond donors

[d]HBA-No. of hydrogen bond acceptors

[e]logPo/w-Predicted Octanol/water partition coefficient

[f] Log S-aqueous solubility of a compound

[g]PCaco-Predicted apparent Caco-2 cell permeability in nm/s

[h]logBB- Predicted brain/blood partition coefficient [i]Rot-No. of rotatable bonds

3.5.7 Result and discussion of *In-silico* prediction of Physico-chemical parameters

Before the approval of the market of any new drugs, the molecules should satisfy the ADMET parameters; if the unit fails in the study, they were removed. *In-silico* prediction of ADMET properties (Absorption, Distribution, Metabolism, and Toxicity) has reduced the effort of the researcher to determine it practically for every designed analog to develop a lead compound.[56] The various physicochemical parameters were predicted, and the results of the parameters (table-2) revealed that most of the compounds satisfied the ideal range of settings such as Mol. Wt. hydrogen bond donors (HBD), hydrogen bond acceptors (HBA), and partition coefficient (log P) were found within the acceptable range and followed Lipinski rule of five as that followed by

95% of the market approved drugs **(Table 3.4)**. Further, five of the titled compounds (Compounds **11b, 11c, 11j, 11k,** and **11l**) showed low values of predicted log S, and their values lied outside the given range (-6.5 to 0.5). So, these five compounds may possess poor aqueous solubility, but for the continuation of SAR studies, we included these compounds for further studies. So overall, based upon the predicted values of these physic-chemical parameters, the majority of compounds possessed the drug-likeness behavior.

3.5.8 Molecular docking studies

Results of docking studies (i.e.) the amino acid residues involved in the various bond formation with the studied ligands and the distances of the interaction exhibited by the ligands are depicted in **table 3.6** and **3.7** respectively.

Table 3.6 Docking analysis of the amino acid residues which place a vital role in the bond-formation with the significantly active and moderately active compounds.

Code (PDB-3MEE)	**H-bond**	**Aromatic bond**	**π-π stacking**	**Glide score (Kcal/mol)**	**Glide energy (Kcal/mol)**
Co-crystal ligand	LYS-101 (2)	HIE-235 LYS-101	-	-14.2	-57.06
Compound – 11J (Significantly active compound)	LYS-101	-	TRP-229 PHE-227	-9.8	-29.4
Compound – 11L (Weakly active compound)	-	-	TRP-229 PHE-227	-7.8	-17.2

Compound code	Atoms which are participating in the interactions			Bond distances (A^o)	Type of bonding
	Atoms of the Ligand molecule	**Atoms of the Amino-acid residue**	**Amino-acid**		
Co-crystal ligand (Rilpivirine)	NH40	O74	LYS-101	2.27	Hydrogen bond
	N2	H815	LYS-101	1.74	Hydrogen bond
	CH42	O74	LYS-101	2.47	Aromatic bond
	CH41	O536	HIE-235	2.58	Aromatic bond
Compound - 11j	OH-43	O74	Lys-101	2.82	Hydrogen bond
Compound-11l exhibited only two π-π interactions					

Table 3.7 Atomic-level interactions and the distances of the significantly active and moderately active compounds with the targeted protein -*3MEE*

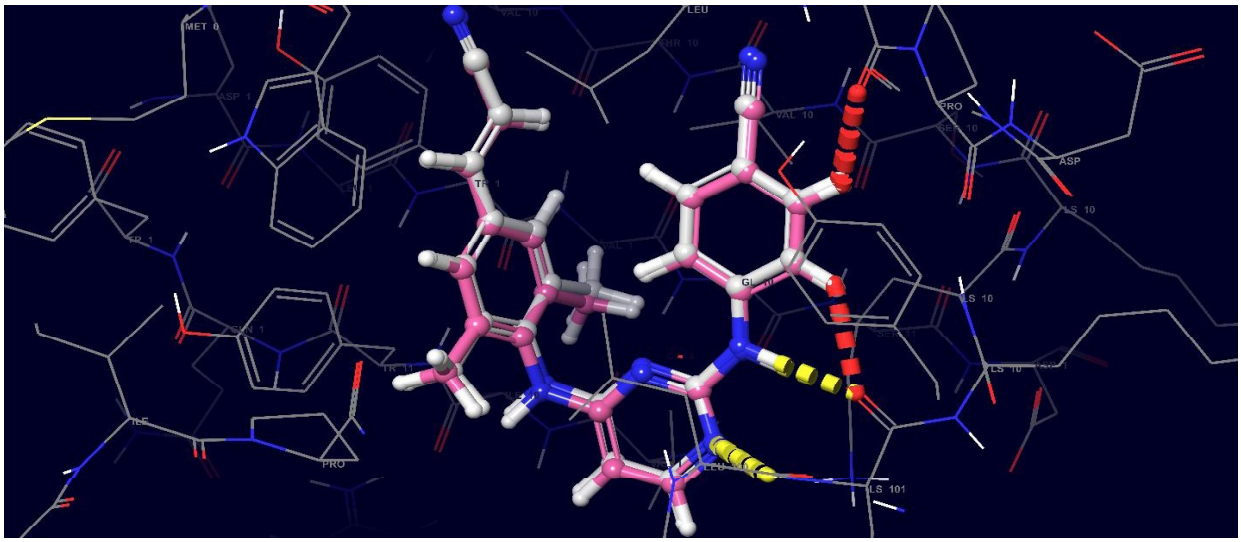

Figure 3.7 Superimposed view of the native pose of ligand (X-Ray crystallized pose) and docked pose of the same ligand in the active site of the protein (3MEE) (Root mean square deviation 0.22A^{O})

[Color interpretation: White – X- Ray crystallized pose, Pink – Docked pose]

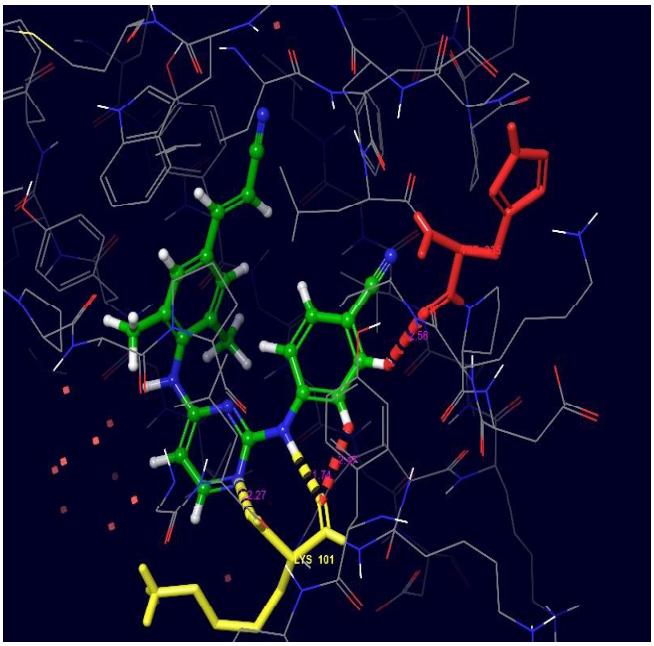

Figure 3.8 Partnership with the co-crystallized ligand exhibited hydrogen, aromatic bond interactions with LYS-101 and HIE-235 in the active site of the protein (3MEE)

[Color interpretation: Yellow- Hydrogen bond, Red- aromatic bond]

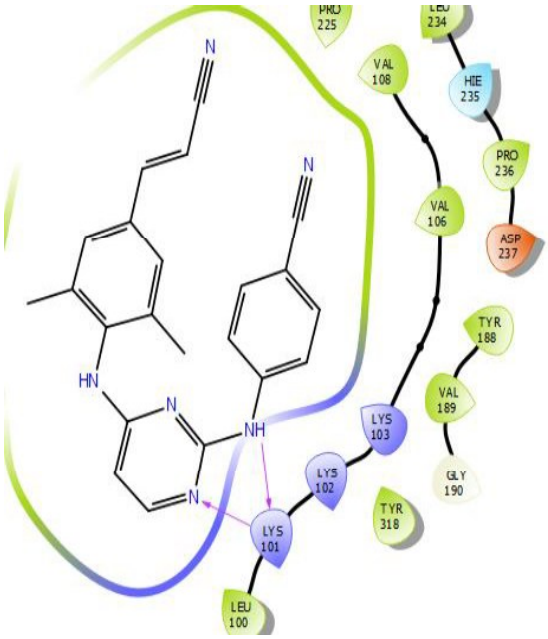

Figure 3.9 2D representation of docked pose of the co-crystallized ligand

[Color interpretation: Magenta- Hydrogen bond]

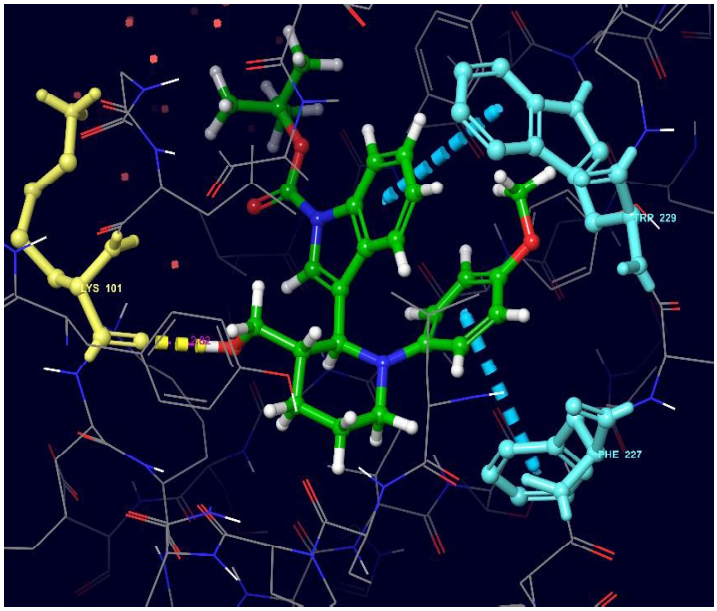

Figure 3.10 Partnership with the significantly active compound 11J exhibited hydrogen bond interaction with LYS-101, Pi-Pi stacking interactions with PHE-227 and TRP-229 in the active site of the protein (3MEE) [Color interpretation: Yellow- Hydrogen bond, Blue- pi-pi stacking]

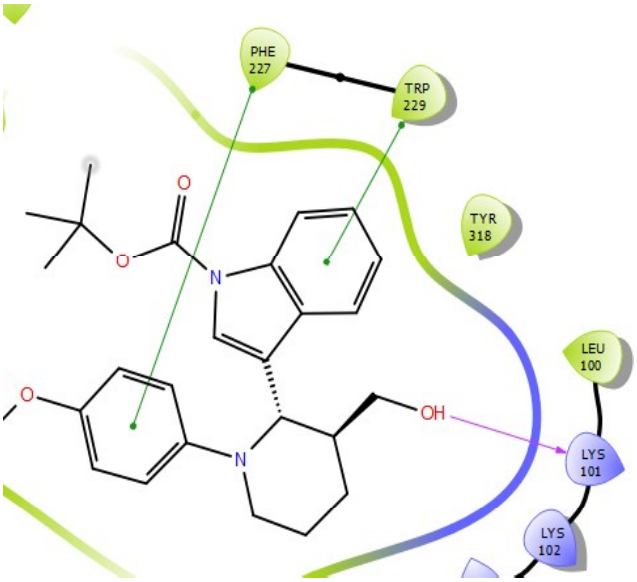

Figure 3.11 2D representation of docked pose of the significantly active compound11J [Color interpretation: Magenta- Hydrogen bond, Green- pi-pi stacking]

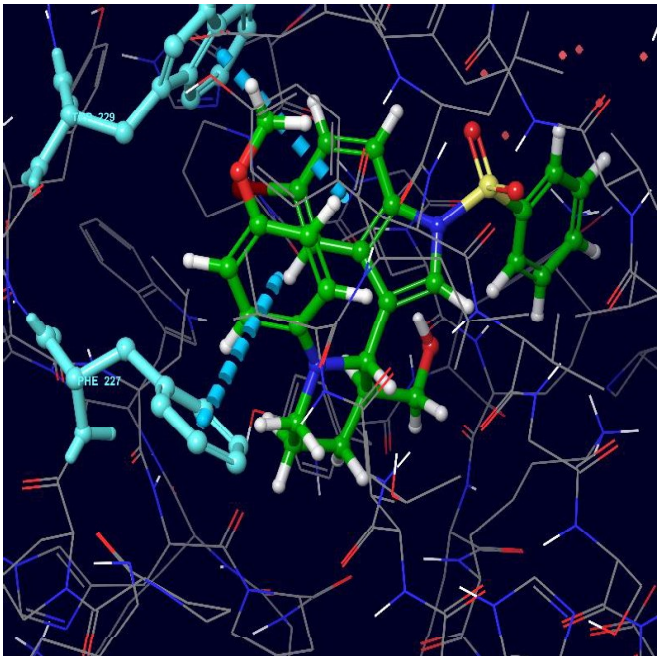

Figure 3.12 Partnership with the weakly active compound 11l exhibited Pi-Pi stacking interactions with PHE-227 and TRP-229 in the active site of the protein (3MEE) [Color interpretation: Blue- pi-pi stacking]

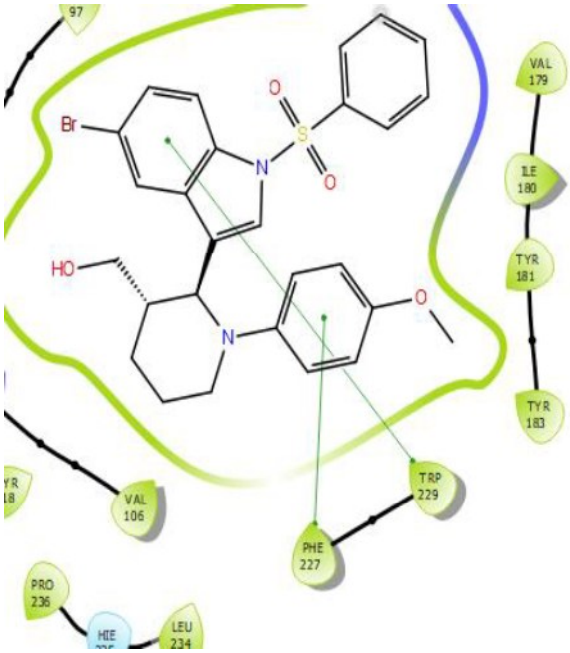

Figure 3.13D representation of docked pose of the weakly active compound 11l [Color interpretation: Green- pi-pi stacking]

3.5.9 Results and discussion of docking studies

Docking studies were carried out by using HIV 1-RT (3MEE) to find the putative binding modes with significantly active and weakly active molecules.[56] Before proceeding for the docking studies, the protein was validated by re-docking of the co-crystallized ligand (Rilpivirine) in the same protein, and the RMSD obtained was 0.22 A^o **(Figure 3.7)**. The RMSD value specified that the docking protocol could be relied on for the docking studies. By examining the 3D docked pose interactions **(Figure 3.8)** and 2D representation **(Figure 3.9)** exhibited by Rilpivirine, LYS-101 showed two hydrogen bonds, HIE-235 and LYS-101 **(Table 3.6)** displayed two aromatic bonds respectively, with the docking score and energy of -14.2 kcal/mol, -57.06 kcal/mol, respectively. The amine nitrogen 40 of Rilpivirine participated in the hydrogen bond interaction with the oxygen 74 of the amino-acid residue LYS-101 with a distance of 2.27 A^o, the same amino-acid residue also exhibited another hydrogen bond interaction with the nitrogen 2 atom of the co-crystallized ligand and hydrogen 815 of the amino-acid residue with the distance of 1.74 A^o **(Table 3.7)**. In addition to this, two aromatic bonds were also observed between CH 41 of rilpivirine and O 74 of the amino-acid residue LYS-101; CH 14 of the co-crystallized ligand and O 536 of the amino-acid residue HIE-235 with the distances of 2.47, 2.58 A^o, respectively.3D docked pose **(Figure 3.10)** and 2D representation **(Figure 3.11)** of significantly active compound 11j presented one hydrogen bond interaction with the amino-acid residue LYS-101 same as that of the co-crystallized ligand with the docking score of -9.8 and energy of -29.40 kcal/mol. Above mentioned hydrogen bond was noticed between OH 43 of the compound 11j and O 74 of the amino-acid residue LYS-101 with a distance of 2.82 A^o. Apart from this, compound 11j also exhibited two π-π stacking interactions with TRP-229 and PHE-227 amino acid residues of the target protein. Thus, compound 11j was well correlated with the *in-vitro* study results and revealed significant % inhibition (70.16%) of HIV-1 RT. While, the 3D docked pose **(Figure 3.12)** and 2D representation **(Figure 3.13)** of the weakly active compound **11l** revealed only two π-π stacking interactions with the amino acid residue TRP-229 and PHE-227 of the target protein with docking score and energy of -7.8 kcal/mol, -17.20 kcal/mol, respectively. Furthermore, it was noteworthy that, compound **11l** does not exhibit any hydrogen bonding interaction with the receptor, so overall weak binding affinity of compound **11l** may be responsible for its less potency against HIV-1 RT (28.48 % inhibition) in the *in vitro* assay compared with the standard drug efavirenz 99.89%.

3.6 Conclusion

In conclusion of this chapter, we have successfully developed a one-pot methodology to synthesized functionalized indol-3-yl piperidine in good yield up to 79% and excellent enantioselectivity (> 99%). This one-pot formal [4+2] cycloaddition/annulation transformation involves direct Mannich reaction of glutaraldehyde **9 (**1,4-carbon *donor-acceptor*) and several indole imines **2** followed by acid-catalyzed $NaBH_4$ reductive cyclization. This chapter also explained the presence of indolyl-tagged piperidine as a basic core in various biologically active natural compounds. *In-vitro* HIV-1 RT inhibitory study and docking study of developed molecules is also an interesting part of the chapter.

3.7.1 Experimental Methods

General Remark: Unless otherwise stated, all reagents were purchased from commercial suppliers and used without further purification. All solvents employed in the reactions were distilled from appropriate drying agents before use. All reactions under standard conditions were monitored by thin-layer chromatography (TLC) on Merck silica gel 60 F254 pre-coated plates (0.25 mm). The column chromatography was performed on silica gel (100-200) using a mixture of hexane/EtOAc. Chemical yields refer to pure isolated substances. ^{1}H-NMR spectra were recorded on a BRUKER-AV400 (400 MHz) spectrometer. Chemical shifts are reported in ppm from tetramethylsilane with the solvent resonance as the internal standard ($CDCl_3$= δ 7.26 for ^{1}H, and 77.0 for ^{13}C-NMR). Data are reported as follows: chemical shift, multiplicity (s = singlet, d = doublet, dd = doublet of doublet, t = triplet, q = quartet, br = broad, m = multiplet), coupling constants (Hz) and integration. ^{13}C-NMR spectra were recorded on a BRUKER-AV400 (75 MHz) spectrometer with complete proton decoupling. HRMS was employing an ESI^+ ionization method and TOF as an analyzer. Infrared (FT-IR) spectra were recorded on an ABB Bomen MB 3000 FTIR Spectrophotometer system using KBr pellets. Melting points were determined in open capillary tubes with an EZ-Melt automated melting point apparatus and may be incorrect.

3.7.2 Typical procedure for the synthesis of indol-3-yl-piperidine

General Experimental Methods

Thin-layer chromatography (on SiO_2 gel F254 plates) was used to observe all reaction under standard conditions. Flash column chromatographic technique was used to purify the compounds

with the help of silica gel (260-400 meshes) and the ratio of hexane-ethyl acetate as the eluting solvent. All reagents used were analytic grade. ^{1}H and ^{13}C NMR study were recorded in $CDCl_3$ as a solvent, and spectral data were reported in ppm relative to tetramethylsilane (TMS) as internal standard, HPLC was performed on Water-2998 Instrument using i-PrOH/Hexane as the solvent system by CHIRALPAK IC columns. HRMS-technique recorded using quadruple electrospray ionization (ESI) technique.

General procedure for Synthesis of one pot indol-3-yl-piperidinevia organocatalysis Mannich reaction followed by $NaBH_4$ reduction as a formal [4+2] cycloaddition:

The glutaraldehyde (extracted from 25% aqueous solution0.9 mmol) was dissolved in 1.5ml DMSO and was added to pre-mixed solution L-proline (20 mol%) and indole imine (0.3 mmol) in DMSO (1.0 mL) and $CHCl_3$ (0.5 mL) (3:1) was added to the mixture at 0°C and stirred at sustain temperature until imine consumed, which was observed by TLC. Once the imine is consumed, carefully $NaBH_4$ portion wise added at 0°C along with few drops of methanol/water and continued the resulting reaction mixture at room temperature for two hours. The reaction was subsequently quenched with $NaHCO_3$ (20% solution 10 mL). The aqueous solution was extracted with ethyl acetate (3 x 10 ml), and combined organic extracts were washed with brine twice, and dried over anhydrous Na_2SO_4 followed by concentrated in vacuum after filtration. The crude product was purified on flash column chromatography on silica gel (100-200 mesh) using hexane-ethyl acetate as eluent to afford indol-3-yl piperidines **(11)** in reported yields.

3.7.3 Analytical data of synthesized compounds (11a-11mand 4)

(1-(4-methoxyphenyl)-2-(1-tosyl-1H-indol-3-yl)piperidin-3-yl)methanol (11a). Red solid,

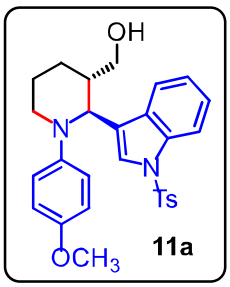

11a

(116 mg, 79% yield, mp = 96-99 °C), $[\alpha]_D^{25}$ = –2.7 (*c* 1.0, $CHCl_3$, er =99.8:0.2).^{1}H NMR (400 MHz, Chloroform-*d*) δ 7.84–7.74 (m, 2H), 7.34 (s, 1H), 7.27 (d, *J* = 8.3 Hz, 2H), 7.22–7.15 (m, 2H), 7.05 (d, *J* = 8.0 Hz, 2H), 6.88 (d, *J* = 8.7 Hz, 2H), 6.53 (d, *J* = 8.7 Hz, 2H), 4.23 (d, *J* = 8.5 Hz, 1H), 3.66 (s, 3H), 3.48 (dd, *J* = 10.6, 4.2 Hz, 1H), 3.36–3.26 (m, 2H), 2.90–2.84 (m, 1H), 2.29 (s, 3H), 2.16–2.10 (m, 1H), 2.02–1.98 (m, 1H), 1.93–1.84 (m, 2H), 1.57–1.49 (m, 1H). ^{13}C NMR (100 MHz, Chloroform-*d*) δ 155.2, 146.1, 144.3, 135.1, 130.1, 129.9, 129.6 (2C), 126.8, 126.3 (2C), 125.3, 124.4, 124.2 (2C), 122.9, 121.1, 113.7 (2C), 113.5, 65.0, 58.8, 56.0, 55.1, 43.0, 26.9, 25.3, 21.5. HRMS (ESI-TOF) *m/z*: [M+H$^+$] Calcd for $C_{28}H_{30}N_2O_4S$ 491.2004, Found 521.2115. Enantiomeric excess was determined by HPLC with a

Chiralpak IC column (*n*-Hexane:*i*-PrOH = 90:10), 0.5 mL/min; major enantiomer t_R = 10.753 min; minor enantiomer t_R = 11.134 min.

(2-(5-chloro-1-tosyl-1H-indol-3-yl)-1-(4-methoxyphenyl)piperidin-3-yl)methanol (11b). Red solid, (112 mg, 71% yield, mp = 102-105°C), $[\alpha]_D^{25}$ = –0.67 (*c* 1.0, $CHCl_3$, er = 97:3). ^{1}H NMR (400 MHz, Chloroform-*d*) δ 7.85 (d, *J* = 2.0 Hz, 1H), 7.68 (d, *J* = 8.8 Hz, 1H), 7.38 (s, 1H), 7.28 (d, *J* = 0.8 Hz, 2H), 7.16 (dd, *J* = 8.8, 2.1 Hz, 1H), 7.09 (d, *J* = 8.5 Hz, 2H), 6.90 (d, *J* = 9.0 Hz, 2H), 6.56 (d, *J* = 9.0 Hz, 2H), 4.18 (d, *J* = 8.8 Hz, 1H), 3.69 (s, 3H), 3.47 (dd, *J* = 10.6, 3.9 Hz, 1H), 3.35–3.26 (m, 2H), 2.87–2.80 (m, 1H), 2.33 (s, 3H), 2.09–2.00 (m, 2H), 1.93–1.86 (m, 2H), 1.63–1.53 (m, 1H).^{13}C NMR (100 MHz, Chloroform-*d*) δ 155.4, 145.9, 144.4, 134.6, 133.4, 131.2, 130.0, 129.7 (2C), 128.8, 126.6, 126.2 (2C), 124.7 (2C), 123.1, 120.9, 114.5, 113.7 (2C), 64.8, 58.8, 56.5, 55.1, 43.8, 27.0, 25.4, 21.5. HRMS (ESI-TOF) *m/z*: [M+H$^+$] Calcd for $C_{28}H_{29}ClN_2O_4S$ 525.1615, Found 521.2115. Enantiomeric excess was determined by HPLC with a Chiralpak IC column (*n*-Hexane: *i*-PrOH = 90:10), 0.5 mL/min; minor enantiomer t_R = 8.860 min; major enantiomer t_R = 10.453 min.5.285 min; major enantiomer t_R = 6.555 min.

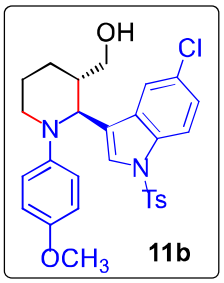

(1-(4-methoxyphenyl)-2-(1-tosyl-1H-indol-3-yl)piperidin-3-yl)methanol (11c). Red solid (123 mg, 72 % yield, mp = 105-107 °C, $[\alpha]_D^{25}$ = –3.3 (*c* 1.0, $CHCl_3$, er = 97.3:2.5). ^{1}H NMR (400 MHz, Chloroform-*d*) δ 7.98 (s, 1H), 7.62–7.59 (m, 1H), 7.33 (s, 1H), 7.26–7.24 (m, 3H), 7.06 (d, *J* = 6.8 Hz, 2H), 6.88–6.86 (m, 2H), 6.54–6.52 (m, 2H), 4.15 (d, *J* = 8.5 Hz, 1H), 3.66 (s, 3H), 3.45–3.42 (m, 1H), 3.31–3.23 (m, 2H), 2.81 (t, *J* = 10.8 Hz, 1H), 2.30 (s, 3H), 2.06–1.86 (m, 4H), 1.56–1.48 (m, 1H). ^{13}C NMR (100 MHz, Chloroform-*d*) δ 155.4, 145.9, 144.7, 134.7, 133.8, 131.7, 129.7 (2C), 127.3, 126.4, 126.2 (2C), 124.6 (2C), 123.9, 123.0, 116.5, 114.9, 113.7 (2C), 64.8, 58.9, 56.4, 55.1, 43.8, 27.0, 25.4, 21.4. HRMS (ESI-TOF) *m/z*: [M+H$^+$] Calcd for $C_{28}H_{29}BrN_2O_4S$ 569.1109, Found 569.1113. Enantiomeric excess was determined by HPLC with a Chiralpak IC column (*n*-Hexane:*i*-PrOH = 90:10), 0.5 mL/min; minor enantiomer t_R = 5.285 min; major enantiomer t_R = 6.555 min.

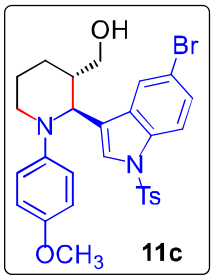

(2-(5-methoxy-1-tosyl-1H-indol-3-yl)-1-(4-methoxyphenyl)piperidin-3-yl)methanol (11d).

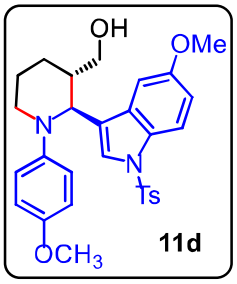

Red solid, (117 mg, 75% yield, mp = 91-94 °C), $[\alpha]_D^{25}$ = –0.9 (*c* 1.0, $CHCl_3$, er = 99.6:0.4). ^{1}H NMR (400 MHz, Chloroform-*d*) δ 7.65 (d, *J* = 9.0 Hz, 1H), 7.30–7.24 (m, 4H), 7.04 (d, *J* = 7.9 Hz, 2H), 6.89 (d, *J* = 8.4 Hz, 2H), 6.80 (dd, *J* = 9.3, 2.4 Hz, 1H), 6.55 (d, *J* = 8.3 Hz, 2H), 4.20 (d, *J* = 8.5 Hz, 1H), 3.81 (s, 3H), 3.67 (s, 3H), 3.50–3.46 (m, 1H), 3.36–3.24 (m, 2H), 2.88–2.82 (m, 1H), 2.30 (s, 3H), 2.13–1.97 (m, 2H), 1.91–1.86 (m, 2H), 1.55–1.51 (m, 1H). ^{13}C NMR (100 MHz, Chloroform-*d*) δ 156.0, 155.2, 146.0, 144.3, 135.0, 131.2, 129.9, 129.6 (2C), 126.2(2C), 126.1, 124.2 (2C), 123.6, 114.3, 113.8 (2C), 113.1, 103.8, 65.0, 58.7, 56.0, 55.6, 55.1, 43.8, 26.9, 25.4, 21.5. HRMS (ESI-TOF) *m/z*: [M+H$^+$] Calcd for $C_{29}H_{32}N_2O_5S$ 521.2110, Found 521.2115. Enantiomeric excess was determined by HPLC with a Chiralpak IC column (*n*-Hexane:*i*-PrOH = 90:10), 0.5 mL/min; major enantiomer t_R = 8.232 min; minor enantiomer t_R = 6.413 min.

3-(3-(hydroxymethyl)-1-(4-methoxyphenyl)piperidin-2-yl)-1-tosyl-1H-indole-5-carbonitrile

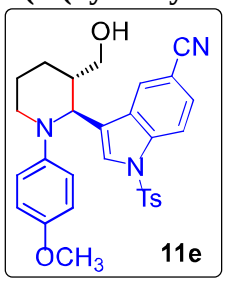

(11e). Red solid, (100 mg, 65% yield, mp= 109-111 °C), $[\alpha]_D^{25}$ = –0.36 (*c* 1.0, $CHCl_3$, er = 99:1). ^{1}H NMR (400 MHz, DMSO-d_6) δ 8.33–8.31 (m, 1H), 7.86 (d, *J* = 8.6 Hz, 1H), 7.73 (s, 1H), 7.61 (dd, *J* = 8.6, 1.6 Hz, 1H), 7.55 (d, *J* = 8.4 Hz, 2H), 7.27 (d, *J* = 8.1 Hz, 2H), 6.94 (d, *J* = 9.0 Hz, 2H), 6.57 (d, *J* = 9.0 Hz, 2H), 4.30 (d, *J* = 8.7 Hz, 1H), 3.58 (s, 3H), 3.20–3.05 (m, 3H), 2.74–2.68 (m, 1H), 2.30 (s, 3H), 1.95–1.85 (m, 3H), 1.79–1.74 (m, 1H), 1.47–1.38 (m, 1H). ^{13}C NMR (100 MHz, Chloroform-*d*) δ 155.4, 145.6, 145.1,136.7, 134.3, 129.8 (2C), 127.3, 127.2, 126.6, 126.2 (2C), 124.8 (3C), 123.2,119.5, 114.1, 113.6 (2C), 106.2, 64.4, 58.7, 56.7, 55.0, 43.7, 26.9, 25.4, 21.4. HRMS (ESI-TOF) *m/z*: [M+H$^+$] Calcd for $C_{29}H_{29}N_3O$516.1957, Found 516.1956. Enantiomeric excess was determined by HPLC with a Chiralpak IC column (*n*-Hexane: *i*-PrOH = 90:10), 0.5 mL/min; minor enantiomer t_R = 6.758 min; major enantiomer t_R = 8.825 min.

(1-(4-methoxyphenyl)-2-(1-(methylsulfonyl)-1H-indol-3-yl)piperidin-3-yl)methanol(11f).

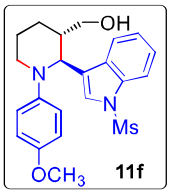

Red solid, (87 mg, 70% yield, mp = 133-136 °C),$[\alpha]_D^{25}$ = –0.23 (*c* 1.0, $CHCl_3$, er = 89.5:10.5).^{1}H NMR (400 MHz, Chloroform-*d*) δ 7.94–7.92 (m, 1H), 7.80–7.77 (m, 1H), 7.28–7.25 (m, 1H), 7.11 (s, 1H), 6.90 (d, *J* = 8.9 Hz, 2H), 6.55 (d, *J* = 8.9 Hz, 2H), 4.20 (d, *J* = 8.7 Hz, 1H), 3.60 (s, 3H), 3.50 (dd, *J* = 10.6, 4.3 Hz, 1H),

3.38 (dd, *J* = 10.6, 5.6 Hz, 1H), 3.26 (m, 1H), 2.89 (m, 1H), 2.59 (s, 3H), 2.22–2.15 (m, 2H), 2.04–1.99 (m, 2H), 1.89–1.84 (m, 2H), 1.56–1.48 (m, 1H). ^{13}C NMR (100 MHz, Chloroform-*d*) δ 155.3, 145.9, 135.6, 130.0, 125.1, 124.8, 124.6 (2C), 124.1, 123.3, 121.6, 113.5 (2C), 113.2, 64.8, 59.3, 55.6, 55.2, 43.4, 39.2, 26.8, 25.2. HRMS (ESI-TOF) *m/z*: [M+H$^+$] Calcd for $C_{22}H_{26}N_2O_4S$ 415.1691, Found 521.2115. Enantiomeric excess was determined by HPLC with a Chiralpak IC column (*n*-Hexane:*i*-PrOH = 92:8), 0.5 mL/min; minor enantiomer t_R = 14.202 min; major enantiomer t_R = 16.127 min.

(2-(5-bromo-1-(methylsulfonyl)-1H-indol-3-yl)-1-(4-methoxyphenyl)piperidin-3-yl)methanol(11g). Red solid, (92 mg, 62% yield, mp = 145-147ºC),$[\alpha]_D^{25}$ = –0.45 (*c* 1.0, $CHCl_3$, er = 90:10).^{1}H NMR (400 MHz, Chloroform-*d*) δ 8.09 (d, *J* = 1.7 Hz, 1H), 7.66 (d, *J* = 8.8 Hz, 1H), 7.37 (dd, *J* = 8.8, 1.7 Hz, 1H), 7.12 (s, 1H), 6.91 (d, *J* = 8.9 Hz, 2H), 6.58 (d, *J* = 8.9 Hz, 2H), 4.13 (d, *J* = 9.1 Hz, 1H), 3.62 (s, 3H), 3.50 (dd, *J* = 10.6, 4.0 Hz, 1H), 3.37 (dd, *J* = 10.6, 5.4 Hz, 1H), 3.26–3.23 (m, 1H), 2.88–2.81 (m, 1H), 2.61 (s, 3H), 2.18–2.00 (m, 3H), 1.93–1.85 (m, 2H), 1.58–1.49 (m, 1H). ^{13}C NMR (100 MHz, Chloroform-*d*) δ 155.7, 145.8, 134.3, 131.7, 127.8, 126.3, 125.1 (2C), 124.4, 123.6, 116.9, 114.8, 113.7 (2C), 64.9, 59.5, 56.1, 55.3, 43.5, 39.6, 27.0, 25.4. HRMS (ESI-TOF) *m/z*: [M+H$^+$] Calcd for $C_{22}H_{25}BrN_2O_4S$ 493.0796, Found 521.2115. Enantiomeric excess was determined by HPLC with a Chiralpak IC column (*n*-Hexane:*i*-PrOH = 90:10), 0.5 mL/min; major enantiomer t_R = 10.748 min; minor enantiomer t_R = 11.403 min.

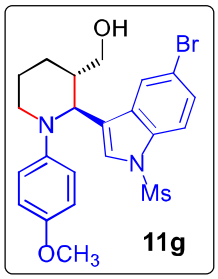

(2-(5-methoxy-1-(methylsulfonyl)-1H-indol-3-yl)-1-(4-methoxyphenyl)piperidin-3-yl) methanol (11h). Red solid (90 mg, 68% yield, mp = 118-120 ºC), $[\alpha]_D^{25}$ = –0.41 (*c* 1.0, $CHCl_3$, er = 93.8:6.2). ^{1}H NMR (400 MHz, Chloroform-*d*) δ 7.67 (d, *J* = 9.0 Hz, 1H), 7.52 (dd, *J* = 5.7, 3.3 Hz, 1H), 7.39 (s, 1H), 7.08 (s, 1H), 6.91–6.88 (m, 2H), 6.58 (d, *J* = 9.0 Hz, 2H), 4.17 (d, *J* = 8.6 Hz, 1H), 3.86 (s, 3H), 3.62 (s, 3H), 3.54 (dd, *J* = 10.6, 4.3 Hz, 1H), 3.41 (dd, *J* = 10.6, 5.4 Hz, 1H), 3.26 (d, *J* = 11.6 Hz, 1H), 2.91–2.83 (m, 1H), 2.54 (s, 3H), 2.21–2.12 (m, 2H), 2.05–2.01 (m, 2H), 1.90–1.86 (m, 2H). ^{13}C NMR (100 MHz, $CDCl_3$) δ 156.4, 155.5, 146.0, 131.3, 130.9, 128.8, 126.1, 124.7 (2C), 114.2, 113.6 (2C), 113.5, 104.4, 65.6, 65.1, 59.3, 55.8, 55.30, 39.0, 30.6, 27.0, 25.4. HRMS (ESI-TOF) *m/z*: [M+H$^+$] Calcd for $C_{23}H_{28}N_2O_5S$ 445.1797, Found 445.1793. Enantiomeric excess was determined by HPLC with a Chiralpak IC column (*n*-

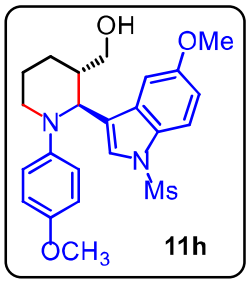

Hexane:*i*-PrOH = 90:10), 0.5 mL/min; minor enantiomer t_R = 6.898 min; major enantiomer t_R = 9.401 min.

3-(3-(hydroxymethyl)-1-(4-methoxyphenyl)piperidin-2-yl)-1-(methylsulfonyl)-1H-indole-5-carbonitrile(11i). Red solid, (88 mg, 67% yield, mp = 132-135°C), $[\alpha]_D^{25}$ = –0.53 (*c* 1.0, $CHCl_3$, er = 92.6:7.4). ^{1}H NMR (400 MHz, $CDCl_3$) δ 8.36 (s, 1H), 7.86 (d, *J* = 8.6 Hz, 1H), 7.51 (d, *J* = 8.6 Hz, 1H), 7.28 (s, 1H), 6.90 (d, *J* = 8.8 Hz, 4H), 6.56 (d, *J* = 8.8 Hz, 4H), 4.22 (d, *J* = 9.0 Hz, 1H), 3.61 (s, 3H), 3.49 (dd, *J* = 10.6, 3.7 Hz, 1H), 3.37–3.33 (m, 1H), 3.27–3.24 (m, 1H), 2.86–2.75 (m, 1H), 2.75 (s, 3H), 2.12–2.00 (m, 2H), 1.95–1.86 (m, 1H), 1.61–1.52 (m, 1H), 1.25 (s, 1H). ^{13}C NMR (100 MHz, Chloroform-*d*) δ 155.6, 145.6, 137.2, 129.9, 127.7, 127.1, 126.9, 125.0 (2C), 123.7, 119.4, 114.0, 113.7 (2C), 106.8, 64.6, 59.2, 56.5, 55.2, 43.5, 40.4, 27.0, 25.4. HRMS (ESI-TOF) *m/z*: [M+H$^+$] Calcd for $C_{23}H_{25}N_3O_4S$ 440.1644, Found 521.2115. Enantiomeric excess was determined by HPLC with a Chiralpak IC column (*n*-Hexane:*i*-PrOH = 92:08), 0.5 mL/min; minor enantiomer t_R = 21.222 min; major enantiomer t_R = 23.701 min.

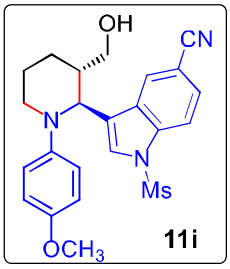

***tert*-butyl-3-((2S,3S)-3-(hydroxymethyl)-1-(4-methoxyphenyl)piperidin-2-yl)-1H-indole-1-carboxylate (11j).** Red solid (84 mg, 64% yield, mp =91-94 °C), $[\alpha]_D^{25}$ = –0.94 (*c* 1.0, $CHCl_3$, er = 99.57:0.43).^{1}H NMR (400 MHz, Chloroform-*d*) δ 7.86 – 7.97 (m, 2H), 7.35 (s, 1H), 7.25 – 7.17 (m, 2H), 6.95 (d, *J* = 9.0 Hz, 2H), 6.61 (d, *J* = 9.0 Hz, 2H), 4.28 (d, *J* = 8.0 Hz, 1H), 3.65 (s, 3H), 3.57 (dd, *J* = 10.7, 4.8 Hz, 1H), 3.44 (dd, *J* = 10.7, 5.6 Hz, 1H), 3.32 – 3.26 (m, 1H), 2.95–2.89 (m, 1H), 2.24–2.18 (m, 1H), 2.05–1.99 (m, 1H), 1.90–1.85 (m, 2H), 1.63 (s, 9H), 1.56–1.48 (m, 1H). ^{13}C NMR (100 MHz, Chloroform-*d*) δ 154.9, 149.7, 146.0, 135.3, 129.5, 124.0 (2C), 123.6 (2C), 122.1, 121.2, 120.9, 115.0, 113.7 (2C), 83.6, 65.2, 58.8, 55.2, 43.3, 29.7, 28.1 (3C), 26.6, 24.9. HRMS (ESI-TOF) *m/z*: [M+H$^+$] Calcd for $C_{26}H_{32}BrN_2O_4$ 437.2740, Found 521.2115. Enantiomeric excess was determined by HPLC with a Chiralpak IC column (*n*-Hexane: *i*-PrOH = 90:10), 0.5 mL/min; major enantiomer t_R = 10.980 min; minor enantiomer t_R = 11.330 min.

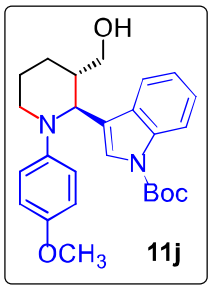

***tert*-butyl-5-bromo-3-(3-(hydroxymethyl)-1-(4-methoxyphenyl)piperidin-2-yl)-1H-indole-1-carboxylate (11k).** Red solid, (102 mg, 66% yield, mp = 97-100 °C), $[\alpha]_D^{25}$ = –0.72 (*c* 1.0, $CHCl_3$, er = 99.2:0.8). ^{1}H NMR (400 MHz, Chloroform-*d*) δ 8.01 (s, 1H), 7.84 (s, 1H), 7.33–7.27 (m, 2H), 6.94 (d, *J* = 8.5 Hz, 2H), 6.62 (d, *J* = 8.5 Hz, 2H), 4.18 (d, *J* = 8.4 Hz, 1H), 3.66 (s,

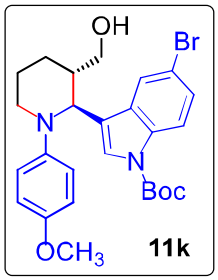

3H), 3.53 (dd, *J* = 10.9, 4.4 Hz, 1H), 3.41 (dd, *J* = 10.7, 5.6 Hz, 1H), 3.23 – 7.28 (m, 1H), 2.86 (td, *J* = 11.9, 11.0, 3.5 Hz, 1H), 2.11 – 2.19 (m, 1H), 2.00 – 2.05 (m, 1H), 1.94–1.84 (m, 2H), 1.62 (s, 9H), 1.56–1.46 (m, 2H). ^{13}C NMR (100 MHz, Chloroform-*d*) δ 155.4, 149.3, 145.9, 131.2, 126.9, 125.2, 124.3 (2C), 123.7, 120.7, 116.4, 115.6, 114.2, 113.8 (2C), 84.1, 65.2, 59.2, 55.8, 55.2, 43.3, 28.2 (3C), 26.8, 25.2. HRMS (ESI-TOF) *m/z*: [M+H$^+$] Calcd for $C_{26}H_{31}BrN_2O_4$ 515.1545, Found 521.2115. Enantiomeric excess was determined by HPLC with a Chiralpak IC column (*n*-Hexane:*i*-PrOH = 90:10), 0.5 mL/min; minor enantiomer t_R = 8.895 min; major enantiomer t_R = 9.906 min.

(2-(5-bromo-1-(phenylsulfonyl)-1H-indol-3-yl)-1-(4-methoxyphenyl)piperidin-3-yl)

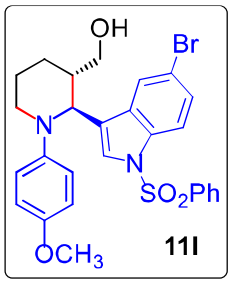

methanol(11l). Red solid, (107 mg, 64% yield, mp = 98-101°C), $[\alpha]_D^{25}$ = –0.59 (*c* 1.0, $CHCl_3$, er = 96.92:3.08). ^{1}H NMR (400 MHz, Chloroform-*d*) δ 7.99 (d, *J* = 1.8 Hz, 1H), 7.64 (d, *J* = 8.8 Hz, 1H), 7.47–7.42 (m, 2H), 7.37 (dd, *J* = 8.6, 1.3 Hz, 2H), 7.33 (s, 1H), 7.30–7.27 (m, 2H), 6.87 (d, *J* = 9.0 Hz, 2H), 6.53 (d, *J* = 9.0 Hz, 1H), 4.15 (d, *J* = 8.8 Hz, 1H), 3.66 (s, 3H), 3.44 (dd, *J* = 10.6, 4.0 Hz, 1H), 3.27 (m, 2H), 2.82 (td, *J* = 11.6, 3.5 Hz, 1H), 2.09–1.96 (m, 3H), 1.91–1.84 (d, *J* = 4.5 Hz, 2H), 1.57–1.57 (m, 2H). ^{13}C NMR (100 MHz, $CDCl_3$) δ 155.5, 145.8, 137.6, 133.9, 133.6, 131.8, 129.1 (2C), 127.5, 126.4, 126.2 (2C), 124.8 (2C), 124.0, 123.2, 116.7, 115.0, 113.8 (2C), 64.8, 59.0, 55.2, 43.8, 29.7, 27.0, 25.4. HRMS (ESI-TOF) *m/z*: [M+H$^+$] Calcd for $C_{27}H_{27}BrN_2O_4S$ 555.0953, Found 521.2115. Enantiomeric excess was determined by HPLC with a Chiralpak IC column (*n*-Hexane:*i*-PrOH = 90:10), 0.5 mL/min; minor enantiomer t_R = 9.117 min; major enantiomer t_R = 10.974 min.

(2-(5-methoxy-1-(phenylsulfonyl)-1H-indol-3-yl)-1-(4-methoxyphenyl)piperidin-3-

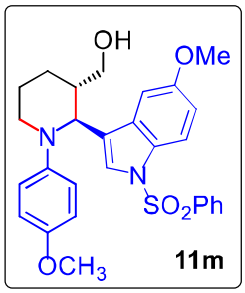

yl)methanol(11m). Red solid, (103 mg, 68% yield, mp = 91-94 °C),$[\alpha]_D^{25}$ = –0.54 (*c* 1.0, $CHCl_3$, er = 95:5)^{1}H NMR (400 MHz, Chloroform-*d*) δ 7.66 (d, *J* = 9.0 Hz, 1H), 7.43–7.35 (m, 3H), 7.30–7.23 (m, 4H), 6.88 (d, *J* = 9.0 Hz, 2H), 6.81 (dd, *J* = 9.0, 2.5 Hz, 1H), 6.53 (d, *J* = 9.0 Hz, 2H), 4.19 (d, *J* = 8.5 Hz, 1H), 3.80 (s, 3H), 3.65 (s, 3H), 3.46 (dd, *J* = 10.6, 4.3 Hz, 1H), 3.32 (dd, *J* = 10.6, 5.4 Hz, 1H), 3.28–3.23 (m, 1H), 2.88–2.81 (m, 1H), 2.12–1.95 (m, 3H), 1.88–1.83 (m, 1H), 1.57–1.50 (m, 1H). ^{13}C NMR (100 MHz, $CDCl_3$) δ 156.09, 155.15, 145.98, 137.80, 133.29, 131.23, 129.88, 128.97, 126.19, 125.98, 124.24, 123.94,

114.35, 113.75, 113.24, 103.89, 64.92, 58.65, 55.65, 55.16, 43.79, 30.97, 26.92, 25.38. HRMS (ESI-TOF) *m/z*: [M+H$^+$] Calcd for $C_{28}H_{30}N_2O_5S$ 507.1953, Found 521.2115. Enantiomeric excess was determined by HPLC with a Chiralpak IC column (*n*-Hexane:*i*-PrOH = 90:10), 0.5 mL/min; minor enantiomer t_R = 9.928 min; major enantiomer t_R = 12.012 min.

(E)-4-(5-methoxy-1-tosyl-1H-indol-3-yl)but-3-en-2-one (4). Color less viscous liquid, (76 mg, 90% yield),[1]H NMR (400 MHz, Chloroform-*d*) δ 7.90 (d, *J* = 9.1 Hz, 1H), 7.86 (s, 1H), 7.78 (d, *J* = 8.4 Hz, 2H), 7.62 (d, *J* = 16.4 Hz, 1H), 7.23 (d, *J* = 8.1 Hz, 2H), 6.78–6.74 (m, 2H), 6.65 (d, *J* = 8.9 Hz, 1H), 3.84 (s, 3H), 2.39 (s, 3H), 2.34 (s, 3H).[13]C NMR (100 MHz, $CDCl_3$) δ 198.1, 156.9, 145.4, 139.9, 134.4, 130.0, 129.95, 129.1, 126.8, 117.9, 116.2, 114.6, 114.5, 114.2, 103.2, 55.7, 27.4, 21.5. HRMS (ESI-TOF) *m/z*: [M+H$^+$] Calcd for $C_{20}H_{19}NO_4S$ 370.1113, Found 370.1095.

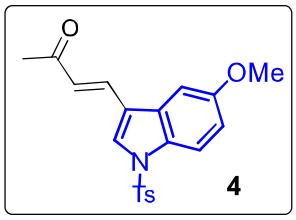

3.8.1 Crystal structure of (2S,3S)-2-(5-bromo-1-(methylsulfonyl)-1H-indol-3-yl)-1-(4-methoxyphenyl)piperidin-3-yl)methanol

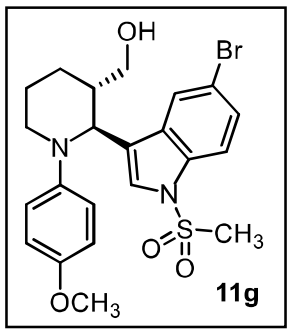

The compound(2S,3S)-2-(5-bromo-1-(methylsulfonyl)-1H-indol-3-yl)1-(4-methoxyphenyl)piperidin-3-yl)methanol($C_{22}H_{25}BrN_2O_4S$) crystallizes in the orthorhombic space group $P2_12_12_1$ with the following unit cell parameters: *a*=12.186(5), *b*=13.146(5), *c*=14.002(5) Å, and Z=4. The crystal structure was solved by direct methods and refined by full matrix least squares procedures to the final R value of 0.044 for 3081 observed reflections. The piperidine ring forms a dihedral angle of 64.60°with the phenyl ring. Piperidine ring adopts chair conformation.

Crystal structure determination and refinement

A crystal of dimensions 0.30 x 0.20 x 0.20 mm was used for data collection on *X*' caliber CCD area-detector diffractometer, equipped with graphite monochromated Mo*Kα* radiation (λ=0.71073 Å). X-ray intensity data consisting of 6286 reflections were collected at 293(2) K and 3970 reflections were found unique. The intensities were measured by scan mode for θ ranges 3.5 to 26.0°. A total number of 3081 reflections were treated as observed [I>2σ(I)]. Data were corrected for Lorentz-polarization and absorption factors. The crystal structure was solved by direct methods using SHELXS97and refined by the full matrix least squares method using

SHELXL97 present in the program suite WinGX. All non-hydrogen atoms of the molecule were located in the best E-map. All the hydrogen atoms were geometrically fixed (except H22) and allowed to ride on the corresponding non-H atoms with C-H= 0.93-0.98 Å and U_{iso} = 1.2 U_{eq}(C), except for the methyl groups where U_{iso}(H) = 1.5U_{eq}(C). The refinement cycles converged the structure to a final *R*- factor of 0.044 (w*R* (F^2) = 0.074) for the 3081 observed reflections. Residual electron densities ranges from -0.283 to 0.486 eÅ^{-3}. Atomic scattering factors were taken from International Tables for X-ray Crystallography. An ORTEP view of the compound with atomic labelling scheme is shown in **Figure 3.14**. The geometry of the molecule was calculated using the PLATON and PARST software. Crystal data, along with data collection and structure refinement details are summarized in **Table 3.8**. Selected bond lengths, bond angles and torsion angles are given in **Table 3.10**.

Table 3.8 Crystal and experimental Data.

Chemical formula	$C_{22}H_{25}BrN_2O_4S$
Crystal system, space group	Orthorhombic, $p2_12_12_1$
Temperature (K)	293
a, *b*, *c* (Å) α, β, γ	12.186 (5), 13.146 (5), 14.002 (5)
V (Å^3)	2243.1 (15)
Z	4
F(000)	1016
D_x (Mg m^{-3})	1.461
Radiation type	Mo *Kα*
No. of reflections for cell measurement	1539
θ range (°) for cell measurement	4.0–24.9
μ (mm^{-1})	1.96
Crystal shape	Block
Colour	Brown
Crystal size (mm)	0.30 × 0.20 × 0.20
Diffractometer	Xcalibur, Sapphire3 diffractometer
Absorption correction	Multi-scan Crys Alis RED
T_{min}, T_{max}	0.864, 1.000
No. of measured, independent and observed [$I > 2\sigma(I)$] reflections	6286, 3970, 3081
R_{int}	0.033
θ values (°)	θ_{max} = 26.0, θ_{min} = 3.5
Range of *h*, *k*, *l*	*h* = −15→15, *k* = −15→16, *l* = −17→10

Refinement	
$R[F^2> 2\sigma(F^2)]$, $wR(F^2)$, S	0.044, 0.082, 1.00
No. of reflections	3970
No. of parameters	278
Restraints	0
$(\Delta/\sigma)_{max}$	0.002
$\Delta\rho_{max}$, $\Delta\rho_{min}$ (e Å^{-3})	0.49, −0.28
Extinction coefficient	0.0012 (3)
Absolute structure parameter	−0.022 (9)

Table 3.9 Selected Bond Distances(Å), Bond Angles (°) and Torsion Angles(°).

Bond lengths		**Bond angles**	
Br—C7	1.904 (4)	C14—O1—H22	124 (10)
O1—C14	1.400 (5)	C18—O2—C21	117.4 (4)
O2—C18	1.361 (5)	C4—N1—C1	107.6 (3)
O2—C21	1.421 (5)	C4—N1—S1	126.4 (3)
O3—S1	1.420 (3)	C1—N1—S1	122.8 (3)
O4—S1	1.423 (4)	C15—N2—C9	115.8 (3)
N1—C4	1.403 (5)	C15—N2—C13	109.5 (3)
N1—C1	1.409 (5)	C9—N2—C13	110.4 (3)
N1—S1	1.665 (4)	O3—S1—O4	120.5 (2)
N2—C15	1.442 (5)	O3—S1—N1	105.6 (2)
N2—C9	1.484 (5)	O4—S1—N1	106.1 (2)
N2—C13	1.485 (5)	O3—S1—C22	109.3 (2)
S1—C22	1.738 (5)	O4—S1—C22	109.3 (2)
		N1—S1—C22	104.9 (2)
		C2—C1—N1	110.8 (4)
		C21—O2—C18—C17	179.8 (4)
		C1—N1—S1—C22	−85.1 (4)
		C5—C6—C7—Br	178.7 (3)

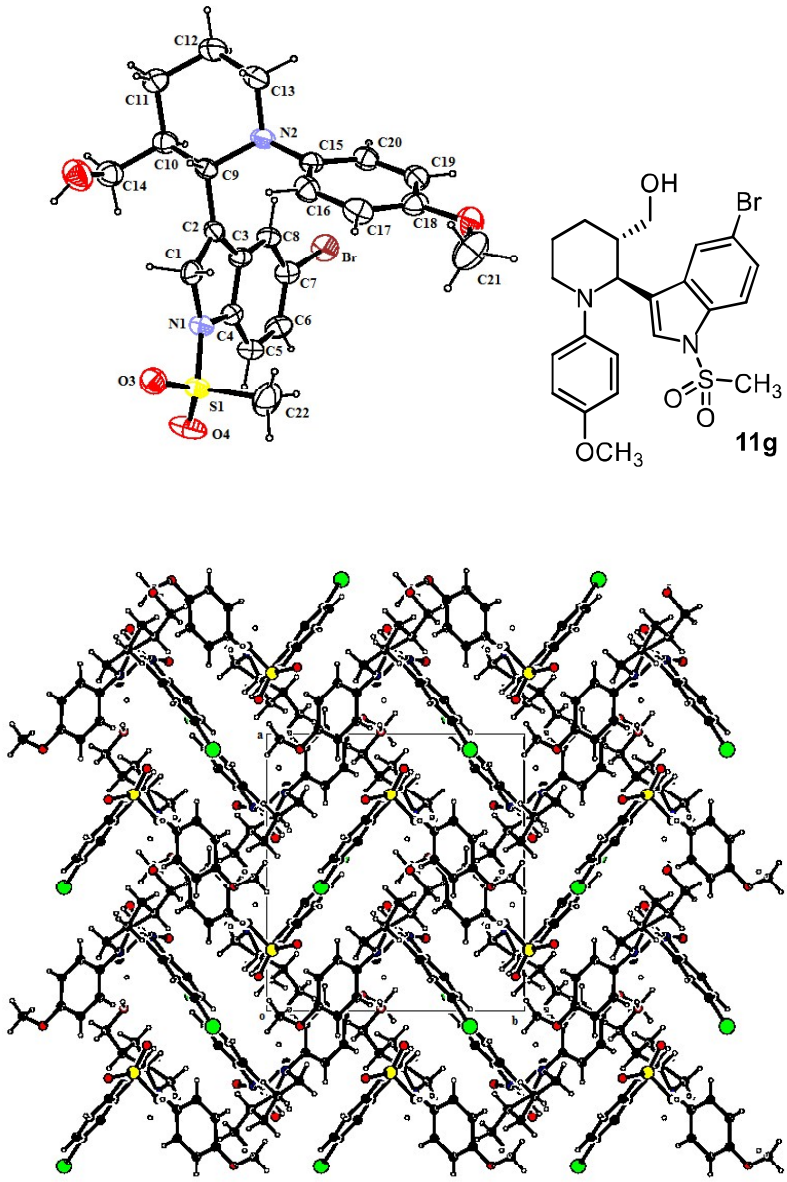

Figure 3.14 *ORTEP* view and atomic labelling of crystal structure of **11g**

Notes and references

[1] Arrayás, R. G.; Carretero. J. C. *Chem. Soc. Rev*. **2009**, *38*, 1940.

[2] Graaff, C. D.; Ruijter, E.; Orru, R. V. A. *Chem. Soc. Rev*. **2012**, *41*, 3969.

[3] Arend, M.; Westermann, B.; Risch, N. *Angew. Chem. Int. Ed*. **1998**, *37*, 1044.

[4] Verkade, J. M. M.; Van Hemert, L. J. C.; Quaedflieg, P. J. L. M.; Rutjes, F. P. J. T. *Chem. Soc. Rev*. **2008**, *37*, 29.

[5] Pellissier, H. *Tetrahedron*. **2007**, *63*, 9267.

[6] Kobayashi, S.; Ishitani, H.; Kobayashi, S.; Ishitani, H. *Chem. Rev*. **1999**, *99*, 1069.

[7] Cordova, A. *Acc. Chem. Res*. **2004**, *37*, 102.

[8] Sharma, V.; Kumar, P.; Pathak, D. *J. Heterocycl. Chem*. **2010**, *47*, 491.

[9] Macor, J. E.; Fox, C. B.; Johnson, C.; Koe, B. K.; Lebel, L. A.; Zorn, S. H. *J. Med. Chem***1992**, *35*, 3625.

[10] Poter, J. K.; Bacon, C. W.; Robins, J. D.; Himmelsbach, D. S.; Higman, H. C. *J. Agric. Food Chem*. **1977**, *25*, 88.

[11] Undberg, R. J. **1996**. The Chemistry of Indoles, p. 113. New York: Academic Press.

[12] Singh, U. P.; Sarma, B. K.; Mishra, P. K.; Ray, A. B. *Fol. Microbiol.* **2000**, *45*, 173–176.

[13] Andreani, A.; Granaiola, M.; Leoni, A.; Locatelli, A.; Morigi, R.; Rambaldi, M.; Giorgi, G.; Salvini, L.; Garaliene, V. *Anticancer Drug. Des*. **2001**, *16*, 167.

[14] Mukhopadhyay, S.; Handy, G. A.; Funayama, S.; Cordell, G. A. *J. Nat. Prod*. **1981**, *44*, 696–700.

[15] Quetin-Leclercq, J. *J. Pharm. Belg*. **1994**, *49*, 181–192.

[16] Sakai, R.; Higa, T.; Jefford, C. W.; Bernardinelli, G.; Manzamine, A. *J. Am. Chem. Soc.* **1986**, *108*, 6404.

[17] Mishra, S.; Ghosh, R. *Tetrahedron Lett*. **2011**, *52*, 2857.

[18] Boswell R.F.; Welstead W. J.; Duncan R. L.; Jonson D. N.; Funderburk W.H. *J. Med. Chem*. **1978**, *21*, 136.

[19] Bariau, A.; Jatoi, W. B.; Calinaud, P.; Troin, Y.; Canet, J. L. *Eur. J. Org. Chem*. **2006**, *2006*, 3421.

[20] Legros, J.; Meyer, F.; Coliboeuf, M.; Crousse, B.; Bonnet Delpon, D.; Begue, J. P. *J. Org. Chem*. **2003**, *68*, 6444.

[21] Mitchinson, A.; Nadin, A. *J. Chem. Soc. Perkin Trans*. **2000**, *1*, 2862.

[22] Weintraub, P. M.; Sabol, J. S.; Kane, J. M.; Borcherding, D. R. *Tetrahedron*. **2003**, *59*, 2953.

[23] Watson, S.; Jiang, B.; Scott, B. *Org. Lett*. **2000**, *2*, 3679

[24] Chen, T.; Xu, X. P.; Ji, S. J. *J. Comb. Chem*. **2010**, *12*, 659.

[25] Dalton King, H.; Meng, Z.; Denhart, D.; Mattson, R.; Kimura, R.; Wu, D.; Gao, Q.; Macor, J. E. *Org. Lett*. **2005**, *7*, 16.

[26] Kinsman, A. C.; Kerr, M. A. *Org. Lett*. **2001**, *3*, 20.

[27] Hanessian, S.; Stoffman, E.; Mi, X.; Renton, P. *Org. Lett*. **2011**, *13*, 5.

[28] Liu, J. F.; Jiang, Z. Y.; Wang, R. R.; Zeng, Y. T.; Chen, J. J.; Zhang, X. M.; Ma, Y. B. *Org. Lett*. **2007**, *9*, 4127.

[29] Zheng, H. Z.; Dong, Z. H.; Yu, Q. *Xueyaun Beijing*.**1997**, *1*, 328.

[30] Rowley, M.; Hallett, D. J.; Goodacre, S. *J. Med. Chem*. **2001**, *44*, 1603.

[31] Rebecca, A. J.; Kudzovi, A. A.; Matthew, G. K.; Stuart, G. G.; Andrew, H. S. Lynn SD International Patent 66126. **2005**.

[32] Matthias, N.; Olivier, R. U S Patent 32976. **2008**.

[33] Li, Z, Zhang, S.; Wu, S.; Shen, X.; Zou, L.; Wang, F.; Li, X.; Peng, F, Zhang, H.; Shao, Z. *Angew. Chem. Int. Ed*. **2013**, *52*, 4117.

[34] Laforteza, B. N.; Pickworth, M.; MacMillan, D. W. C. *Angew. Chem. Int. Ed*. **2013**, *52*, 11269.

[35] Frei, R.; Staedler, D.; Raja, A.; Franke, R.; Sasse, F.; GerberLemaire, S. *Angew. Chem*. **2013**, *125*, 13615.

[36] Frei, R.; Staedler, D.; Raja, A.; Franke, R.; Sasse, F.; Lemaire, S. G.; Waser, J. *Angew. Chem. Int. Ed*. **2013**, *52*, 13373.

[37] Wei, Yi.; Zhao, D.; Ma, D. *Angew. Chem. Int. Ed*. **2013**, 52, 12988.

[38] Rowley, M.; Hallett, D. J.; Goodacre, S.; Moyes, C.; Crawforth, J.; Sparey, T. J.; Patel, S.; Marwood, R.; Patel, S.; Thomas, S.; Hitzel, L.; Connor, D. O.; Szeto, N.; Castro, J. L.; Hutson, P. H.; MacLeod, A. M. *J. Med. Chem*. **2001**, *44*,1605.

[39] Xie, L. H.; Cheng, J.; Luo, Z. W.; Lu, G. *Tetrahedron Letters*. **2018**, *59*, 4571.

[40] Kumar, I.; Ramaraju, P.; Mir, N. A.; Singh, D.; Gupta, V. K.; *K*ant, R. *Chem. Comm.* **2013,** *49*, 5645.

[41] Ramaraju, P.; Mir, N. A.; Singh, D.; Kumar, I. *RSC adv*. **2016**, *6*, 60422.

[42] Ramaraju, P.; Mir, N. A.; Singh, D.; Sharma, P.; Kant, R.; Kumar, I. *Eur. J. Org. Chem*. **2017**, 3461.

[43] Ramaraju, P.; Mir, N. A.; Singh, D.; Gupta, V. K.; Kant, R.; Kumar, I.*Org. Lett*. **2015,***17*, 5582.

[44] Eberle, J.; Knopf, C. W. *Methods in Enzymology*. **1996**, *275*, 257.

[45] Chander, S.; Ashok, P.; Zheng, Y. T.; Wang, P.; Raja, K. S.; Taneja, A.; Murugesan, S. *Bioorganic Chemistry*. **2016**, *64*, 66.

[46] Schrödinger Release. **2019**-1: Maestro, Schrödinger, LLC, New York, NY, 2019.

[47] Schrödinger Release. **2019**-1: QikProp, Schrödinger, LLC, New York, NY, 2019.

[48] Jorgensen, W. L.; Maxwell, D. S.; Tirado-Rives, J. *J. Am. Chem. Soc.* **1996**, *118*, 11225.

[49] Schrödinger Release. **2019**-1: LigPrep, Schrödinger, LLC, New York, NY, 2019.

[50] Burley, S. K.; Berman, H. M.; Bhikadiya, C.; Bi, C.; Chen, L.; Di Costanzo, L.; Christie, C.; Dalenberg, K.; Duarte, J. M.; Dutta, S. *Nucleic Acids Res.* **2019**, *47*, D464.

[51] Schrödinger Release **2019**-1: Schrödinger Suite 2019-1 Protein Preparation Wizard; Epik, Schrödinger, LLC, New York, NY, 2019.

[52] Lansdon, E. B.; Brendza, K. M.; Hung, M.; Wang, R.; Mukund, S.; Jin, D.; Birkus, G.; Kutty, N.; Liu, X. *J. Med. Chem.* **2010**, *53,* 4295.

[53] Friesner, R. A.; Banks, J. L.; Murphy, R. B.; Halgren, T. A.; Klicic, J. J.; Mainz, D. T.; Repasky, M. P.; Knoll, E. H.; Shelley, M.; Perry, J. K. *J. Med. Chem.* **2004**, *47*, 1739.

[54] Manual, Q. U.; Manual, Q. U. QikProp Descriptors and Properties PISA. **2015**, 2.

[55] Ashok, P.; Sharma, H.; Lathiya, H.; Chander, S.; Murugesan, S. *Med. Chem. Res.* **2015**, *24*, 513.

[56] Chander, S.; Wang, P.; Ashok, P.; Yang, L. M.; Zheng, Y. T.; Sankaranarayanan, M. *Bioorg. Med. Chem. Lett.* **2017**, *27*, 61.